

A PRIMER ON THE NONLINEAR SCHRÖDINGER EQUATION

by

Ole Krarup

© Ole Krarup, Vejle, Denmark

Contents

Table of Contents	ii
List of Figures	v
List of Tables	ix
1 Introduction	1
1.1 Goal	1
1.2 Availability	2
1.3 Citation Policy	2
1.3.1 On citing this primer	2
2 Math and Theory	4
2.1 Real and Complex fields	4
2.1.1 Actual electric field and the electric field envelope	5
2.2 Fourier Transform	6
2.3 Pulses	7
2.4 Chrip and Delay	7
3 Attenuation and Gain	9
3.1 Physical origins of attenuation	9
3.2 Describing attenuation	9
3.3 The dB scale	10
3.4 Measuring power in dBm	11
3.5 Common dB and dBm mistakes	11
4 Dispersion	13
4.1 Pulses and spatial frequency	13
4.2 β_0 - How much the carrier gets delayed	15
4.2.1 Phase velocity	15

4.3	β_1 - How much the envelope of a pulse centered at the carrier gets delayed	16
4.4	β_2 - How much the frequencies constituting the envelope of a pulse centered at the carrier get delayed relative to each other	16
4.4.1	The "Zero Dispersion Frequency"	18
4.5	β_n - Higher order delays	18
4.6	Are $\alpha(\omega)$ and $\beta(\omega)$ independent?	19
5	Self Phase Modulation	21
5.1	Phase change across pulse	21
5.2	Spectral broadening	23
5.3	SPM, Attenuation and "Effective Length"	23
5.4	Self-Strengthening	25
5.4.1	Applicability	26
6	Four Wave Mixing	28
6.1	Electrical phase modulation	28
6.2	Nonlinearity based phase modulation	29
6.3	Cross Phase Modulation (XPM)	32
6.4	Phase matching	35
6.4.1	Modulation Instability	35
7	The Raman effect	38
7.1	The Raman response function	38
7.1.1	Expressions for $h_R(T_{\text{delay}})$	40
8	Exotic pulses	43
8.1	The Fundamental Soliton	43
8.1.1	Solitons in telecommunications	44
8.2	Higher order Solitons	44
8.2.1	Soliton fission	44
8.3	Optical Wave Breaking	47
8.3.1	Similaritons	47
8.4	Novel Solitons	49
8.4.1	Dark Solitons	49
8.4.2	Raman Solitons	49
8.4.3	Vector Solitons	49

9 Supercontinuum Generation	52
9.1 Case study	52
9.2 Your turn!	52
10 Recommended material	56
10.1 Optics	56
10.2 Electronics	57
10.3 Communication	58
10.4 Simulation tools	58
Bibliography	60

List of Figures

- | | |
|---|----|
| 4.1 a) A pulse with a long duration compared to the duration of a single electric field oscillation at the carrier frequency will have a narrow spectrum. b) Conversely, a short pulse will have a wide spectrum. | 14 |
| 4.2 Illustration of the effect of different β_n terms on a Gaussian pulse in the time domain. Left column shows a comparison of the power envelope of the pulse before and after propagating through media with different β_n terms. Right column shows the evolution of the power envelope with distance. a) Medium with $\beta_2 < 0$. b) Medium with $\beta_3 > 0$. c) Medium with $\beta_4 < 0$. d) Medium where $\beta_2 < 0$, $\beta_3 > 0$ and $\beta_4 < 0$ are present simultaneously. Figures generated using the numerical simulation in this interactive notebook, which the reader is encouraged to experiment with. | 20 |
| 5.1 Visualization of the impact of SPM on a) a Gaussian pulse, b) a triangular pulse, c) a square pulse, d) an arbitrary pulse. In general, positive slopes result in a red-chirp, decreasing slope leads to a blue-chirp and horizontal slopes result in no chirp. | 22 |
| 5.2 Before-and-after comparison of a Gaussian pulse propagating through a nonlinear medium described by Eq. 5.1. a) In the time domain, the power envelope of the pulse is unchanged. b) The spectrum broadens. c) Evolution of the power envelope in the time domain exhibits no change. d) The spectrum gradually broadens. e) Spectrogram of pulse before propagation. f) Spectrogram of pulse after propagation. Note the broadening in the spectral domain and constant width in the temporal domain. Figures generated using the numerical simulation in this interactive notebook, which the reader is encouraged to experiment with. | 24 |

5.3 Before-and-after comparison of a Gaussian pulse propagating through a nonlinear medium described by Eq. 5.9. a) In the time domain, the power envelope of the pulse becomes steeper in the back because the peak of the pulse experiences a higher refractive index due to the nonlinearity and slows down. b) The spectrum broadens asymmetrically towards higher frequencies due to the steep, decreasing slope in the back. c) Evolution of the power envelope in the time domain. d) The spectrum gradually broadens towards higher frequencies. e) Spectrogram of pulse before propagation. f) Spectrogram of pulse after propagation. Figures generated using the numerical simulation in this interactive notebook, which the reader is encouraged to experiment with.

27

6.1 Illustration of the impact of electrical sinusoidal phase modulation of a continuous wave optical signal. Before entering the modulator, only a single laser frequency is present. After the modulator, the alternating advancement and delay of the optical phase in the time domain is equivalent to introducing new frequency components according to Eq. 6.2. 30

6.2 a) Numerically calculated initial and final spectrum when two frequencies with $P_b = 100P_a$ spaced 5 GHz apart propagate through a medium where $\phi_{NL} = 2\gamma L \sqrt{P_a P_b} = 1.08$ rad. Note the transfer of power from the most intense frequency into neighbouring sidebands and the rapid decrease in power for increasing sideband orders as predicted by Eq. 6.9. b) Same as a) but for $\phi_{NL} = 2\gamma L \sqrt{P_a P_b} = 7.2$ rad. c) Comparison of sideband power normalized to P_b according to numerical simulations and Eq. 6.8. d) Similar to c) but plotted on a double-log scale versus ϕ_{NL} to demonstrate the scaling behavior predicted by Eq. 6.9. Figures generated using this interactive notebook, which the reader is encouraged to experiment with.

33

6.3 Illustration of the disparate impacts of SPM and XPM on the phase of an optical signal. a) Time domain representation of a low power CW signal overlapped with two identical, high power Gaussian pulses that only differ by their carrier frequencies. The carrier frequency of the pulse on the left is 10 GHz below the carrier frequency of the CW light. b) After simulating the propagation through a nonlinear medium, the CW light obtains approximately twice the phase shift from XPM as from SPM as predicted by Eq. 6.14. The ratio of $0.0360/0.0187 \approx 1.925 \neq 2$ is attributed to the approximations involved in Eq. 6.14 and to the finite time resolution of the simulation. Figures generated using this interactive notebook, which the reader is encouraged to experiment with.	34
6.4 a) Initial and final time domain power of a signal consisting of a Gaussian pulse and random noise with an amplitude 1.000 times smaller than that of the Gaussian propagated through 100m of a nonlinear medium with $\beta_2 < 0$. b) Same as a) but showing the spectrum. c-d) Same as a-b) but for a distance of 200m. e-f) Same as a-b) but for a distance of 300m. g) full temporal evolution for 500m. h) Same as g) but for the spectrum. Figures generated using this interactive notebook, which the reader is encouraged to experiment with.	37
7.1 a) Graphs of Eq. 7.6 (green), Eq. 7.7 (red) and Eq. 7.8 (purple) in the time domain. b) Imaginary part of the Fourier Transform of the functions plotted in a). c) Initial and final spectrum of a pulse subjected to SPM only. d) Initial and final spectrum for the same pulse as in c) subjected to the Raman effect described by Eq. 7.6. Note the asymmetric broadening skewed to lower frequencies as predicted by the analysis of Eq. 7.5. e) Same as d) but for Eq. 7.7 f) Same as d) but for Eq. 7.8. Figures generated using this interactive notebook, which the reader is encouraged to experiment with.	42
8.1 Comparison of a Gaussian pulse to a hyperbolic-secant pulse on a linear scale in a) and a logarithmic scale in b), which emphasizes the comparatively more intense tails of the hyperbolic-secant.	45

8.2	a) Temporal evolution of an $N = 3$ soliton for which $A_{max} = 3A_{char} = 3\sqrt{ \beta_2 /\gamma T_0^2}$. The length of the fiber has been chosen to equal the oscillation period of the soliton. b) Spectrum evolution of the $N = 3$ soliton. c-d) Respectively, the temporal and spectral evolutions of the same $N = 3$ soliton as in a-b), but where the fiber has $\beta_3 > 0$, causing the pulse to "fission", thereby illustrating the unstable nature of solitonic propagation. Figures generated using the numerical simulation in this interactive notebook, which the reader is encouraged to experiment with.	46
8.3	a) Evolution of a hyperbolic secant pulse through a medium where $\beta_2 > 0$. b) Evolution of the same pulse as in a) through a medium where $\beta_2 > 0$ and $\gamma > 0$ cause power to "pile up" in the front and back of the pulse, leading to OWB. c) Same conditions as in b), but where $\alpha > 0$ causes a triangular pulse to evolve towards a parabola. Figures generated using the numerical simulation in this interactive notebook, which the reader is encouraged to experiment with.	48
8.4	a) Fundamental dark soliton propagating stably through a medium where $\beta_2 > 0$ and $\gamma > 0$. b) An $N=3$ dark soliton propagating through the same medium as in a) Instead of stable propagation, the central dip gives rise to additional ones. c) An $N=3$ soliton propagating through a medium where $\beta_2 < 0$ and $\gamma > 0$. d) The same pulse as in c) propagating through the same medium except the Raman effect described by Eq. 7.6 is taken into account, causing soliton fission and a self-redshifting Raman soliton to arise. Figures generated using this interactive notebook, which the reader is encouraged to experiment with.	50
9.1	a) Comparison of the characteristic lengths resulting from the parameters listed in Tab. 9.2. Effects with short characteristic lengths are expected to become significant first. b) Temporal evolution of the pulse showing soliton fission at a distance of around 1 m followed by FWM and the generation of a Raman soliton walking off to later times. c) Spectral evolution of the pulse. d) Initial spectrogram of the pulse at $z=0$ m. e) Final spectrogram at $z=5$ m. The "parabolic" shape arises because $\beta_3 > 0$ ensures that both red and blue light experience time delays compared to the carrier. The bright spot at (0.75 ps, 265 THz) is a Raman soliton. Figures generated using the numerical simulation presented in this interactive notebook, which the reader is encouraged to experiment with.	54

List of Tables

3.1 Examples of scaling factors and corresponding changes measured in dB.	10
7.1 Table of parameters of the exact expression for the Raman response of silica in Eq. 7.8 modified from [1].	41
9.1 Summary of the impacts of different linear and nonlinear effects.	53
9.2 Simulation parameters used for generating a supercontinuum taken from [2]	53

Chapter 1

Introduction

The Nonlinear Schrödinger Equation (NLSE) in its generalized, scalar form describes how the normalized envelope $\mathbf{A} = \mathbf{A}(z, T)$ of the complex electric field $\mathbf{E} = \mathbf{E}(z, T) = \mathbf{E}_0 \cdot \exp(-i(\beta(\omega_0)z - \omega_0 T))$, oscillating with a carrier angular frequency, ω_0 , and carrier spatial frequency $\beta(\omega_0)$, evolves as it propagates through a medium, where attenuation, dispersion and a χ^3 nonlinearity are present. Mathematically, it is given by

$$\partial_z \mathbf{A} = \frac{\alpha}{2} \mathbf{A} + i \sum_{n=2}^{\infty} i^n \frac{\beta_n}{n!} \partial_T^n \mathbf{A} + i\gamma \left(1 + \frac{i}{\omega_0} \partial_T\right) \left(\mathbf{A} \int_0^{\infty} R(T_{\text{delay}}) |\mathbf{A}(z, T - T_{\text{delay}})|^2 dT_{\text{delay}} \right), \quad (1.1)$$

where α is the power attenuation/gain coefficient, $\beta_n = \partial_{\omega}^n \beta(\omega)|_{\omega=\omega_0}$ are the coefficients of the Taylor expansion of the spatial frequency evaluated at $\omega = \omega_0$, γ is the nonlinearity parameter and $R(T_{\text{delay}})$ is the temporal response function of the nonlinearity at a time delay, T_{delay} , before the present time, T . Solving Eq. 1.1 allows one to describe supercontinuum generation [3, 4], solitons [5, 6], nonlinear noise in fiber telecommunications systems [7] and other exotic optical phenomena with a plethora of scientific and industrial applications.

1.1 Goal

This primer explores the constituent terms of Eq. 1.1 and their interactions in a way that aims to develop an intuitive understanding of the mathematics and the underlying physics. To achieve this goal, discussions of more complicated effects, such as those involving the polarization of light, are omitted in favour of more detailed derivations and examples of purely scalar effects. Hopefully, this approach provides

the reader, with the basic tools needed for analyzing common experimental results in nonlinear optics and tackling more advanced resources, papers and textbooks on the topic.

1.2 Availability

This primer is freely available on [GitHub](#) and continuously updated by the author in response to reader feedback. Readers are encouraged to submit questions, tips and suggestions to YourFavouriteTA@gmail.com.

1.3 Citation Policy

This primer cites both original academic works on the explored topics, and links to items such as YouTube videos, personal web pages, online encyclopedia entries, interactive tools and similar material produced by hobbyists and professional researchers alike. The aim is to both provide the reader with a starting point for a comprehensive review of the formal literature necessary for independently writing a paper or thesis on nonlinear optics and a collection of high-quality, accessible explanations to deepen their understanding.

1.3.1 On citing this primer

This primer contains no original research on the NLSE and should be viewed as a collection of detailed notes. It should not be cited as a source when writing a paper or thesis presenting new research on the NLSE. Instead, please cite the oldest original works on relevant topics, such as [5] and [6] in the case of solitons. However, if the aim is simply to familiarize readers with the NLSE to help them grasp original research on it, this primer can be cited in BibTeX format as [8]:

```
@misc{NLSE_primer,  
author = "O. Krarup",  
title = "{A Primer on the Nonlinear Schrödinger Equation}",  
note = "Commit SHA: 9f1b93a",  
url      = {https://github.com/OleKrarup123/NLSE-  
primer/blob/main/NLSE_primer.pdf}}
```

Note that because this primer is freely available on GitHub and is continuously updated, the URL should link to the most recent version, while the "Commit SHA" should be that of the most recent commit the citation is made.

Chapter 2

Math and Theory

This chapter explains the basic mathematical tools needed for describing electromagnetic waves and understanding Eq. 1.1.

2.1 Real and Complex fields

A particle with a charge, q , and mass, m , which is subjected to an electric field $\bar{\mathbf{E}}_r = \mathbf{E}_r \hat{x}$ will experience an acceleration given by

$$\bar{a} = \frac{q\mathbf{E}_r}{m} \hat{x}. \quad (2.1)$$

The subscript, r , on the electric field indicates that this is the "real" electric field which determines how charged particles accelerate. The "complex" electric field is a mathematical tool that makes calculations involving electromagnetic waves easier and from which the real electric field can always be recovered. For example, the real electric field wave propagating through a bulk medium, where its spatial angular frequency, β , depends on the temporal angular frequency, ω , is given by

$$\begin{aligned} \mathbf{E}_r(z, t) &= |\mathbf{E}_0| \cos(\beta(\omega)z - \omega t + \phi) \\ &= |\mathbf{E}_0| \Re \{ \exp(i\beta(\omega)z - i\omega t + i\phi) \} \\ &= \Re \{ \mathbf{E}_0 \exp(i\beta(\omega)z - i\omega t) \} \\ &= \Re \{ \mathbf{E}(z, t) \} \\ &= \frac{1}{2} (\mathbf{E}(z, t) + \mathbf{E}^*(z, t)). \end{aligned} \quad (2.2)$$

For an illustration of Eq. 2.2, see [this interactive graph](#).

Use of the complex electric field is convenient when modelling the effects of phase shifts and interference. For example, to introduce a phase shift of ϕ_0 into the real

field, it must be "inserted manually" by writing

$$\begin{aligned}\mathbf{E}_r(z, t) &= |\mathbf{E}_0| \cos(\beta(\omega)z - \omega t + \phi) \Rightarrow \\ \mathbf{E}'_r(z, t) &= |\mathbf{E}_0| \cos(\beta(\omega)z - \omega t + \phi + \phi_0^\checkmark).\end{aligned}\quad (2.3)$$

Using the complex field, the same operation can be done by using complex multiplication, since

$$\begin{aligned}\mathbf{E}(z, t) &= \mathbf{E}_0 \exp(i\beta(\omega)z - i\omega t + i\phi) \Rightarrow \\ \mathbf{E}'(z, t) &= \mathbf{E}_0 \exp(i\beta(\omega)z - i\omega t + i\phi) \exp(i\phi_0) \\ &= \mathbf{E}_0 \exp(i\beta(\omega)z - i\omega t + i\phi + i\phi_0) \\ \mathbf{E}'_r(z, t) &= \Re \{\mathbf{E}'(z, t)\}.\end{aligned}\quad (2.4)$$

Additionally, since the instantaneous power of an oscillating, real electric field is proportional to its square, the average power over one cycle can either be computed from an integral or from half of the absolute square of the complex electric field,

$$\begin{aligned}\langle \mathbf{E}_r^2 \rangle_T &= \frac{1}{T} \int_0^T \mathbf{E}_r^2 dt = \langle \Re \{\mathbf{E}\}^2 \rangle_T = \frac{1}{4} \langle (\mathbf{E} + \mathbf{E}^*)^2 \rangle_T \\ &= \frac{1}{4} \langle \mathbf{E}^2 + \mathbf{E}^{*2} + 2|\mathbf{E}|^2 \rangle_T = \frac{1}{2} \langle |\mathbf{E}|^2 \rangle_T = \frac{1}{2} |\mathbf{E}|^2.\end{aligned}\quad (2.5)$$

The convenience of replacing both "manual insertion" and integrals by complex multiplication is great enough that doing calculations using the complex electric field and only extracting the real field when necessary is worthwhile. Therefore, this primer primarily utilizes complex fields, but emphasizes that these are only useful mathematical abstractions, while the real fields have physical significance as they directly determine the acceleration of charges.

2.1.1 Actual electric field and the electric field envelope

Radio signals used for Wi-Fi have carrier frequencies of around 5 GHz, while state of the art oscilloscopes can measure fields oscillating at 100 GHz. For comparison, the electric fields of laser pulses typically oscillate at carrier frequencies above 100 THz. Therefore, doing calculations with and expressing results in terms of the actual, complex electric field, $\mathbf{E}(z, t) = \mathbf{E}_0 \exp(i\beta(\omega_0)z - i\omega_0 t)$, is often inconvenient because the fast electric field oscillations occurring $\omega_0/2\pi$ times per second cannot be detected anyways. Instead, one can define the envelope of the complex electric field as

$$A(z, t) = a \cdot \mathbf{E}(z, t) \cdot e^{-i(\beta(\omega_0)z - \omega_0 t)}, \quad (2.6)$$

and use it for calculations instead. Here, $a = \sqrt{0.5\epsilon_0 n c A_{eff}}$, where ϵ_0 is the vacuum permittivity, n is the refractive index of the medium, c is the speed of light and A_{eff} is the effective area of the cross-section of the optical field is a normalization constant. Scaling E by a ensures that A has units of \sqrt{W} , and thus that $|A|^2$ has units of W . By "factoring out" the rapid and undetectable but also *predictable* temporal and spatial oscillations, determining how the electric field *changes* due to linear and non-linear effects becomes easier. See [this interactive graph](#) for an illustration of the difference between E and A .

2.2 Fourier Transform

In this primer, the Fourier transform and its inverse are defined as

$$\begin{aligned}\tilde{E}(z, \omega) &= \mathfrak{F}\{E(z, t)\} = \int_{-\infty}^{\infty} E(z, t) e^{i\omega t} dt, \\ E(z, t) &= \mathfrak{F}^{-1}\{\tilde{E}(z, \omega)\} = \frac{1}{2\pi} \int_{-\infty}^{\infty} \tilde{E}(z, \omega) e^{-i\omega t} d\omega.\end{aligned}\quad (2.7)$$

The convention of using $\exp(i\omega t)$ in the Fourier transform as opposed to $\exp(-i\omega t)$ is chosen because complex plane wave propagating in the forward z-direction are described by $\exp(i\beta(\omega_0)z - i\omega_0 t)$. Thus, the calculation,

$$\begin{aligned}\mathfrak{F}\{\exp(i\beta(\omega_0)z - i\omega_0 t)\} &= \int_{-\infty}^{\infty} e^{i\beta(\omega_0)z - i\omega_0 t} e^{i\omega t} dt, \\ &= \int_{-\infty}^{\infty} e^{i\beta(\omega_0)z - i(\omega_0 - \omega)t} dt \\ &= e^{i\beta(\omega_0)z} \delta(\omega - \omega_0),\end{aligned}\quad (2.8)$$

shows that the Fourier transform of a complex plane wave yields a delta function centered at the positive carrier angular frequency, ω . Using $\exp(-i\omega t)$ in the Fourier transform and applying it to a complex plane wave propagating in the positive z-direction would have yielded a result containing $\delta(\omega_0 + \omega)$, implying that the delta function is centered at the negative carrier angular frequency. The latter approach makes accounting for the sign in calculations involving the Fourier transform of complex plane waves propagating in the z-direction more complicated. Therefore the former convention is used.

2.3 Pulses

Electromagnetic pulses with a finite duration in a medium can be viewed as an infinite sum of distinct complex plane waves as follows

$$\begin{aligned}\textcolor{red}{E}(z, t) &= \frac{1}{2\pi} \int_{-\infty}^{\infty} |\tilde{E}(z, \omega)| e^{i\beta(z, \omega)z - i\omega t + i\phi(z, \omega)} d\omega \\ \textcolor{red}{E}(z, t) &= \frac{1}{2\pi} \int_{-\infty}^{\infty} \tilde{E}(z, \omega) e^{i\beta(z, \omega)z - i\omega t} d\omega.\end{aligned}\quad (2.9)$$

The crucial insight provided by Eq. 2.9 is that any change in the intensity, shape and color of an optical signal must arise from altering the amplitudes, $|\tilde{E}(z, \omega)|$, phases, $\phi(z, \omega)$, or spatial frequencies, $\beta(z, \omega)$, of a set of temporal frequency components. Even nonlinear effects, which can change laser pulses in surprising ways, essentially do nothing more than alter these three parameters.

2.4 Chrip and Delay

Consider the complex electric field at $z = 0$ given by

$$a\textcolor{red}{E}(t) = \textcolor{red}{A}(t) \exp\left(-i\left(\omega_0 + \frac{C}{2}T\right)T\right). \quad (2.10)$$

If $C = 0$, the phase of the field changes linearly, which implies that it oscillates with a fixed carrier frequency of ω_0 . If $C > 0$, Eq. 2.10 suggests that the carrier frequency will increase over time, while $C < 0$ would imply that the carrier frequency decreases. See [this interactive graph](#) for an illustration. The "instantaneous angular frequency" of an electric field is

$$\delta\omega(T) = -\partial_T\phi(T), \quad (2.11)$$

where $\phi(T)$ is the phase of the field as a function of time. The negative in front of the derivative w.r.t. time is included to ensure that the instantaneous angular frequency of a complex plane waves propagating in the z-direction, which is described by $\exp(i\beta(\omega_0)z - i\omega_0 t)$, is correctly calculated to be $+\omega_0$.

An electric field whose instantaneous frequency changes over time is said to be "chirped". Durations, where it oscillates at a frequency lower(higher) than its carrier frequency are said to be "red-chirped"("blue-chirped"). A chirp that changes from "red" to "blue", is said to be "increasing", while a chirp that changes from "blue" to "red" is said to be "decreasing".

Understanding that different durations of a known field can have different instantaneous frequencies, and that these frequencies can be obtained from Eq. 2.11 by computing the negative derivative of the phase of the field is crucial to making sense of a number of linear and nonlinear effects. For example, if the speed of light in a particular medium is such that higher frequencies (i.e. "more blue" ones) propagate faster than lower frequencies (i.e. "more red" ones), an optical pulse propagating through this material will develop a blue chirp in the front and a red chirp in the back.

Just as taking the derivative of the temporal phase w.r.t. time yields information about the instantaneous frequency, one can take the derivative of the spectral phase w.r.t. frequency to determine the time delay of a particular frequency. Consider the spectrum of the complex field envelope at $z = 0$ given by

$$\tilde{A}(\omega) = \tilde{A}_0(\omega) \exp\left(i\left(\frac{B}{2}(\omega - \omega_0)^2\right)\right). \quad (2.12)$$

Assuming $B > 0$, Eq. 2.12 implies that the phases of the frequency components surrounding the carrier angular frequency, ω_0 , increase quadratically with increasing separation from the carrier. Alternatively, one can interpret Eq. 2.12 as stating that the phase *decreases* with frequency for angular frequencies below ω_0 and *increases* with frequency for angular frequencies above ω_0 . Inspired by Eq. 2.11, we can compute

$$\delta t(\omega) = \partial_\omega \phi(\omega), \quad (2.13)$$

which for Eq. 2.12 yields

$$\delta t(\omega) = B(\omega - \omega_0), \quad (2.14)$$

which suggests that angular frequencies below ω_0 experience a negative time shift (causing them to occur earlier), while angular frequencies above ω_0 experience a positive time shift (equivalent to a delay). Note that no change of sign is required in Eq. 2.13 to achieve consistency.

Compared to Eq. 2.11, Eq. 2.13 is less useful for calculations, but the insight that decreasing phase w.r.t. angular frequency implies an early arrival time, while an increasing phase w.r.t. angular frequency implies delayed arrival is helpful when the impact of dispersion is analyzed in Ch. 4. See also [this video tutorial](#) for an illustration of the relationship between changing spectral phase and time delay.

Chapter 3

Attenuation and Gain

Light propagating through a glass medium will naturally experience attenuation as impurities or lattice defects can scatter part of the electromagnetic field away from the original direction of propagation. Because nonlinear optical effects become less significant if the intensity of the light is low, understanding the impact of attenuation is important for understanding Eq. 1.1.

3.1 Physical origins of attenuation

When light propagates in a waveguide, such as an optical fiber, attenuation can occur due to chemical impurities in the glass, crystal defects in the lattice or tight bends in the waveguide. Additionally, if the carrier frequency of the light matches the vibration frequency of a chemical bond in the crystal lattice, light can be converted directly into heat. See [this video series](#) for an intuitive picture of how light propagates through an ideal medium.

3.2 Describing attenuation

Consider Eq. 1.1 where all parameters except for α is equal to zero. In that case,

$$\begin{aligned}\partial_z \mathbf{A} &= \frac{\alpha}{2} \mathbf{A} \\ \mathbf{A}(z, T) &= \mathbf{A}(0, T) \exp\left(\frac{\alpha}{2} z\right).\end{aligned}\tag{3.1}$$

When $\alpha < 0$, Eq. 3.1 implies that the field will attenuate with distance, while $\alpha > 0$ implies that the field experiences gain. Note that the power of the field is proportional

Scaling factor	0.01	0.05	0.1	0.125	0.25	0.4	0.5	0.8	1	1.25	2	2.5	4	8	10	20
dB change	-20	-13	-10	-9	-6	-4	-3	-1	0	1	3	4	6	9	10	13

Table 3.1: Examples of scaling factors and corresponding changes measured in dB.

to the absolute square of the field, so

$$P(z, t) = |\mathbf{A}(z, t)|^2 = |\mathbf{A}(0, t)|^2 \exp(\alpha z). \quad (3.2)$$

In Eq. 1.1, Eq. 3.1 and Eq. 3.2, α is the "power attenuation coefficient", which determines by how many factors of e the *power* of the field has changed after propagating a certain distance. Other authors define α to be the "field attenuation coefficient", which determines by how many factors of e the *field* has changed after propagating a certain distance, in which case Eq. 3.2 would contain $2\alpha z$ in the exponential instead of αz .

3.3 The dB scale

In practical applications, it's common to report attenuation or gain in units of "Decibels" (dB). For example, if a signal initially has 60 mW of power and only, 130 μ W after propagating through a medium, its power has changed by

$$\Delta P[dB] = 10 \log_{10} \left(\frac{P_{final}}{P_{initial}} \right) = 10 \log_{10} \left(\frac{0.130mW}{60mW} \right) = -26.64dB. \quad (3.3)$$

Conversely, if the power is then boosted by 15dB, the new power is

$$P_{final} = P_{initial} \cdot 10^{\frac{\Delta dB}{10}} = 0.13mW \cdot 10^{\frac{15}{10}} = 4.11mW. \quad (3.4)$$

Note that $10 \log_{10}(10) = 10$ dB, $10 \log_{10}(0.1) = -10$ dB, $10 \log_{10}(2) \approx 3$ dB and $10 \log_{10}(0.5) \approx -3$ dB. Thus, if the power is scaled up by a factor of 20 = 10 · 2, this corresponds to an increase of $10 \log_{10}(10 \cdot 2) = 10 \log_{10}(10) + 10 \log_{10}(2) = 13$ dB. See Tab. 3.1 for more examples.

The attenuation coefficient, α is often reported in dB/km. For example, single-mode optical fibers for telecommunications have typical attenuation coefficients of -0.22 dB/km near 193 THz (corresponding to approximately 1550 nm). This implies that a 100km long fiber will change the optical power by -22 dB, which corresponds to a reduction by a factor of approximately 158.5. If $\alpha = -0.22$ dB/km, the appropriate value of α measured in "factors of e per km" to use in Eq. 1.1 (assuming that z is

measured in units of km) can be calculated from

$$\begin{aligned} \exp(\alpha_{\text{Factors of } e \text{ per km}} z) &= 10^{\frac{\alpha_{dB/km}}{10} z} \\ \alpha_{\text{Factors of } e \text{ per km}} z &= \ln\left(10^{\frac{\alpha_{dB/km}}{10} z}\right) \\ &= \frac{\alpha_{dB/km}}{10} z \ln(10) \\ \alpha_{\text{Factors of } e \text{ per km}} &= 0.23 \cdot \alpha_{dB/km} \\ \alpha_{\text{Factors of } e \text{ per km}} \cdot 4.343 &= \alpha_{dB/km}. \end{aligned} \quad (3.5)$$

3.4 Measuring power in dBm

The powers of optical signals are often reported in units of "dBm", which represents the power in decibels relative to "mW". For example, 40 mW corresponds to

$$P[dBm] = 10 \cdot \log_{10} \left(\frac{40mW}{1mW} \right) = 16dBm, \quad (3.6)$$

and conversely,

$$P[mW] = 10^{\frac{16dBm}{10}} mW = 40mW. \quad (3.7)$$

Using "dBm" is convenient as weak signals that are nevertheless detectable can be a few nW, while the peak powers of pulses that have undergone, for example, **chirped pulse amplification** can reach MW or even GW [9]. It also makes accounting for the impact of attenuation and gain easier than using Eq. 3.4 because a signal with an initial power of 0.13 mW = -8.86 dBm, which gets amplified by 15 dB will have a final power of $-8.86 dBm + 15 dB = 6.13 dBm$.

3.5 Common dB and dBm mistakes

- Adding dBm to dBm:** Alice wants to determine the total power of two lasers in dBm. She measures the power of the first laser to be 3dBm and the power of the second laser to be 6dBm.

x Alice calculates $P_{tot}[dBm] = 3dBm + 6dBm = 9dBm$. This is wrong because 3 dBm = 2 mW and 6 dBm = 4 mW, but 9 dBm = 8 mW and because adding dBm values directly corresponds to multiplying the powers measured in linear units: $2 mW \cdot 4 mW = 8 mW^2$!

- ✓ Alice first converts the two measurements to linear units ($3 \text{ dBm} = 2 \text{ mW}$, $6 \text{ dBm} = 4 \text{ mW}$). She then adds the linear values to obtain a total power of 6 mW and finally converts this result to dBm: $10 \cdot \log_{10}(6\text{mW}/1\text{mW}) = 7.78 \text{ dBm}$.

2. Confusing dB and dBm: Bob, wants to know the power of a certain laser in mW. A colleagues of his reports that he has measured the power to be "13 dB".

- ✗ Bob plugs the value of 13 dB into Eq. 3.7 instead of 16 dBm and gets the result 20 mW . This is wrong because "13 dB" is a unitless ratio and not a measure of power!
- ✓ Bob asks his colleague to clarify if he actually meant "13 dBm". The colleague may simply have misspoken, but it's also possible that the display on his power meter actually did say "13 dB" because it was accidentally set to report the current power compared to some previously specified value.

3. More confusion of dB and dBm: Charlie has measured the power of a laser to be 10 dBm . His colleague asks him to reduce the power by "3 dBm".

- ✗ Charlie adjusts the output power from 10 dBm down to 7 dBm . This is wrong because he has cut the power by 3 dB , while a reduction by "3 dBm" would correspond to 2 mW .
- ✓ Charlie asks his colleague to clarify if she meant 3 dB or actually did request a reduction by 2 mW . The former is the most likely situation as the latter (while strictly speaking not incorrect) would be unconventional and potentially confusing use of terminology.

4. Incorrect averaging: David wants to determine the average power in dBm of three lasers whose individual powers are -1 dBm , 4 dBm and 6 dBm .

- ✗ David computes $P_{avg} = (-1 \text{ dBm} + 4 \text{ dBm} + 6 \text{ dBm})/3 = 4 \text{ dBm}$. Doing so does not yield the "regular" average, but the **geometric average** of the three values: $(-1 \text{ dBm} + 4 \text{ dBm} + 6 \text{ dBm})/3 = (0.79 \text{ mW} \cdot 2.51 \text{ mW} \cdot 7.94 \text{ mW})^{1/3} = 2.5 \text{ mW} = 4 \text{ dBm}$. This value can be informative in some situations, but it's not the "regular average" that David is currently interested in! Verifying that power averages are computed consistently is important, for example when a big team is working on characterizing the performance of an optical product they wish to sell!
- ✓ David converts the three powers to linear units, and computes the average as $(0.79 \text{ mW} + 2.51 \text{ mW} + 7.94 \text{ mW})/3 = 3.75 \text{ mW} = 5.74 \text{ dBm}$.

Chapter 4

Dispersion

In the context of optics, "Dispersion" refers to the fact that the speed of light waves in materials such as glass depends on the temporal frequency of those waves. If a beam of light containing multiple different temporal frequencies enters a block of glass at an angle, the constituent frequencies will disperse spatially according to Snell's Law [10]. If a laser pulse with a certain duration consisting of a range of temporal frequencies enters the same block of glass at a right angle, a longer pulse may exit in the other end because the different frequencies of light have taken different amounts of time to propagate through it. This chapter explains how the impact of dispersion on laser pulses can be understood from first principles.

4.1 Pulses and spatial frequency

Consider Eq. 2.9 under the assumption that the pulse is propagating in a spatially homogeneous medium, so that $\beta(z, \omega) = \beta(\omega)$,

$$\textcolor{red}{E}(z, t) = \frac{1}{2\pi} \int_{-\infty}^{\infty} \tilde{E}(z, \omega) e^{i\beta(\omega)z - i\omega t} d\omega. \quad (4.1)$$

In a bulk medium, $\beta(\omega) = n(\omega)\omega/c$, where $n(\omega)$ is the refractive index of the material and c is the speed of light. For a waveguide such as an optical fiber, $\beta(\omega)$ must be determined by solving Maxwell's equations as explained in this [video tutorial](#). Additionally, the durations of the envelopes of pulses considered in this primer are assumed to be much longer than the duration of a single oscillation at their carrier frequencies, $\omega_0/2\pi \approx 200$ THz as illustrated in Fig. 4.1 a).

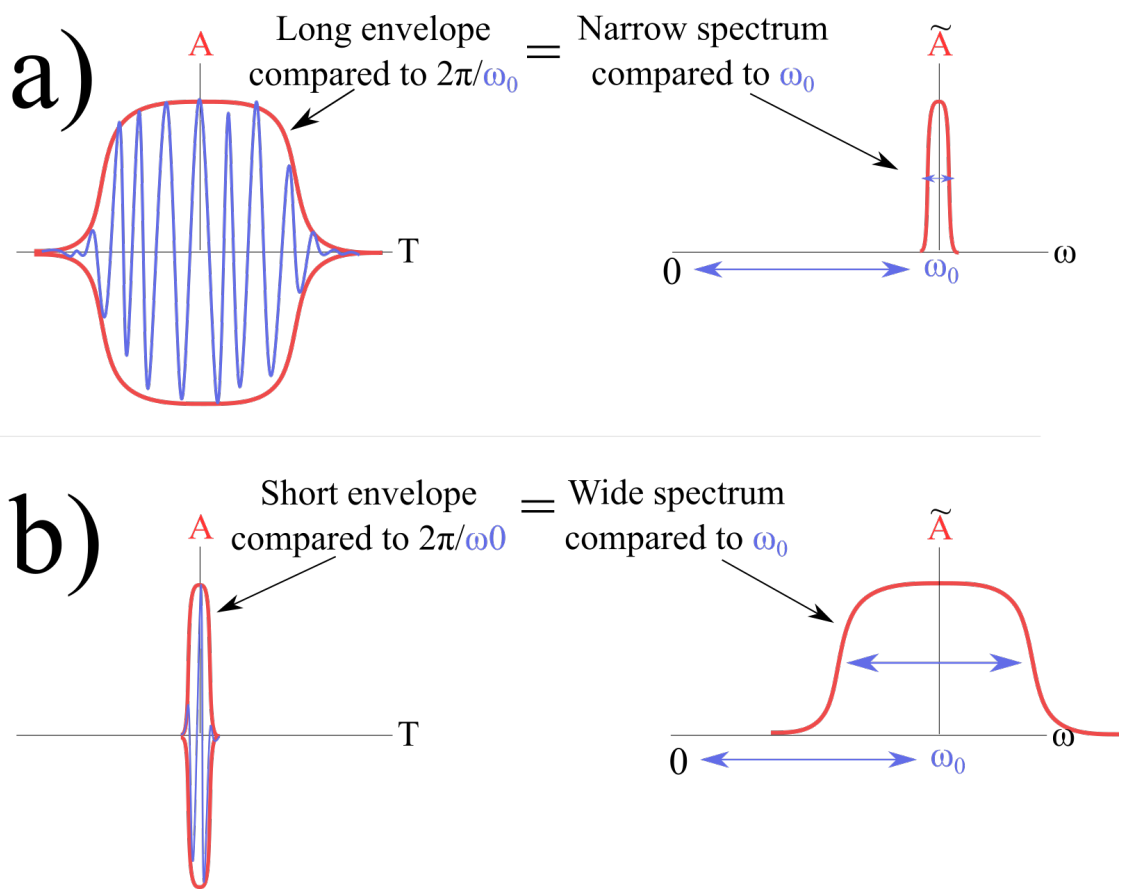


Figure 4.1: a) A pulse with a long duration compared to the duration of a single electric field oscillation at the carrier frequency will have a narrow spectrum. b) Conversely, a short pulse will have a wide spectrum.

Under these assumptions, the spectral width of the pulse is so narrow that $\beta(\omega)$ can be Taylor-approximated around the carrier frequency as

$$\begin{aligned}\beta(\omega) &\approx \beta(\omega_0) + \partial_\omega \beta|_{\omega_0} (\omega - \omega_0) + \frac{1}{2!} \partial_\omega^2 \beta|_{\omega_0} (\omega - \omega_0)^2 + \frac{1}{3!} \partial_\omega^3 \beta|_{\omega_0} (\omega - \omega_0)^3 + \dots \\ &= \sum_{n=0}^{\infty} \frac{1}{n!} \partial_\omega^n \beta|_{\omega_0} (\omega - \omega_0)^n \\ &= \sum_{n=0}^{\infty} \frac{1}{n!} \beta_n (\omega - \omega_0)^n.\end{aligned}\tag{4.2}$$

With this simplification in mind, the expression for a pulse propagating through a medium becomes

$$E(z, t) = \frac{1}{2\pi} \int_{-\infty}^{\infty} \tilde{E}(z, \omega) e^{i(\beta_0 + \beta_1(\omega - \omega_0) + \frac{1}{2}\beta_2(\omega - \omega_0)^2 + \dots)z - i\omega t} d\omega.\tag{4.3}$$

4.2 β_0 - How much the carrier gets delayed

Because the term containing β_0 does not depend on ω , it can be moved outside the integral in Eq. 4.4. Multiplying by $1 = \exp(-i\omega_0 t) \exp(i\omega_0 t)$ yields

$$E(z, t) = \frac{1}{2\pi} e^{i\beta_0 z - i\omega_0 t} \int_{-\infty}^{\infty} \tilde{E}(z, \omega) e^{i(\beta_1(\omega - \omega_0) + \frac{1}{2}\beta_2(\omega - \omega_0)^2 + \dots)z - i(\omega - \omega_0)t} d\omega.\tag{4.4}$$

The exponential outside the integral implies that if one observes the complex electric field in the medium over a duration consisting of a few cycles of the carrier, it will look like a complex plane wave with a temporal frequency of ω_0 and a spatial frequency of β_0 . See [this interactive graph](#) for an illustration of the impact of β_0 on the propagation of a real plane wave in a medium.

4.2.1 Phase velocity

The carrier wave will peak when $\beta_0 z - \omega_0 t$ is an integer multiple of 2π . Consider for simplicity the peak corresponding to $\beta_0 z - \omega_0 t = 0$. If time advances by $0 < \Delta t$, the original value of z does not satisfy $\beta_0 z - \omega_0(t + \Delta t) = 0$. Instead, the peak will be at some new location $z + \Delta z$, where

$$\beta_0(z + \Delta z) - \omega_0(t + \Delta t) = 0\tag{4.5}$$

$$\beta_0 \Delta z - \omega_0 \Delta t = 0.$$

Since the peak has shifted by Δz during the time Δt , one can define the "phase velocity" (or alternatively the "carrier velocity") as

$$v_p = \frac{\Delta z}{\Delta t} = \frac{\omega_0}{\beta_0}. \quad (4.6)$$

4.3 β_1 - How much the envelope of a pulse centered at the carrier gets delayed

The integral in Eq. 4.4 represents the envelope of the complex electric field propagating through the medium. Rearranging the exponential terms, one obtains

$$\mathbf{E}(z, t) = \frac{1}{2\pi} e^{i\beta_0 z - i\omega_0 t} \int_{-\infty}^{\infty} \tilde{\mathbf{E}}(z, \omega) e^{i\beta_1(\omega - \omega_0)z - i(\omega - \omega_0)t} e^{i(\frac{1}{2}\beta_2(\omega - \omega_0)^2 + \dots)z} d\omega. \quad (4.7)$$

Applying the same analysis behind Eq. 4.6, one finds that the peak of the envelope of the complex electric field propagates at the so-called "group velocity" (or alternatively the "envelope velocity") given by

$$v_g = \frac{(\omega - \omega_0)}{\beta_1 \cdot (\omega - \omega_0)} = \frac{1}{\beta_1} = \frac{1}{\partial_{\omega} \beta}. \quad (4.8)$$

See [this interactive graph](#) for an illustration of the difference between phase- and group velocity. Note that Eq. 4.8 agrees with the prediction of Eq. 2.13 that a large, positive change in the phase w.r.t. ω should lead to a large delay.

4.4 β_2 - How much the frequencies constituting the envelope of a pulse centered at the carrier get delayed relative to each other

Applying Eq. 2.6 to Eq. 4.7 allows one to "factor out" the fast but predictable spatial and temporal oscillations of the carrier and focus on the envelope:

$$\mathbf{A}(z, t) = \frac{1}{2\pi} \int_{-\infty}^{\infty} \tilde{\mathbf{A}}(z, \omega) e^{i\beta_1(\omega - \omega_0)z - i(\omega - \omega_0)t} e^{i(\frac{1}{2}\beta_2(\omega - \omega_0)^2 + \dots)z} d\omega. \quad (4.9)$$

To simplify further, one can define $T = t - \beta_1 z$, which is the "time relative to the moment at which the envelope of the pulse arrives at a distance z ". Using T instead of t is convenient because many optics experiments involve sending pulses of light through a medium with a fixed length and tracking the measured power over time

after the light leaves the medium:

$$\begin{aligned}\mathbf{A}(z, T) &= \frac{1}{2\pi} \int_{-\infty}^{\infty} \tilde{\mathbf{A}}(z, \omega) e^{i\beta_1(\omega - \omega_0)z - i(\omega - \omega_0)(T + \beta_1 z)} e^{i(\frac{1}{2}\beta_2(\omega - \omega_0)^2 + \dots)z} d\omega \quad (4.10) \\ &= \frac{1}{2\pi} \int_{-\infty}^{\infty} \tilde{\mathbf{A}}(z, \omega) e^{i(\frac{1}{2}\beta_2(\omega - \omega_0)^2 + \dots)z - i(\omega - \omega_0)T} d\omega.\end{aligned}$$

As explained via Eq. 2.12, a positive(negative) value of β_2 implies that lower(higher) temporal frequencies propagate faster than higher(lower) temporal frequencies, causing the envelope of the pulse to broaden in the time domain. Alternatively, one can consider Eq. 1.1 with only the β_2 term,

$$\partial_z \mathbf{A} = -i \frac{\beta_2}{2} \partial_T^2 \mathbf{A}, \quad (4.11)$$

which is identical to the so-called "Heat Equation" [11, 12]. See also [this tutorial](#). To obtain $\mathbf{A}(z, T)$ given $\mathbf{A}(z = 0, T)$ and thus $\tilde{\mathbf{A}}(z = 0, \omega)$, first compute the Fourier Transform of Eq. 4.11 to obtain

$$\begin{aligned}\partial_z \tilde{\mathbf{A}} &= -i \frac{\beta_2}{2} (i(\omega - \omega_0))^2 \tilde{\mathbf{A}} \quad (4.12) \\ &= i \frac{\beta_2}{2} (\omega - \omega_0)^2 \tilde{\mathbf{A}} \\ \tilde{\mathbf{A}}(z, \omega) &= \tilde{\mathbf{A}}(0, \omega) e^{i \frac{\beta_2}{2} (\omega - \omega_0)^2 z} \\ \mathbf{A}(z, T) &= \mathfrak{F}^{-1} \left\{ \tilde{\mathbf{A}}(z, \omega) \right\}.\end{aligned}$$

For a Gaussian pulse, Eq. 4.12 can be solved [analytically](#). The result indeed implies that the pulse will broaden temporally, while Eq. 2.11 applied to the result confirms that $\beta_2 > 0$ implies that lower frequencies will arrive earlier than higher frequencies. Because the magnitude of the phase shift caused by β_2 grows quadratically with the distance between a given frequency component and the carrier, shorter pulses with greater spectral widths will temporally broaden more over the same distance than shorter ones with smaller bandwidths. A characteristic length over which the broadening due to β_2 becomes significant can be defined as

$$L_2 = \frac{T_0^2}{|\beta_2|}. \quad (4.13)$$

See [this video](#) for an illustration of the impact of dispersion on a Gaussian pulse.

4.4.1 The "Zero Dispersion Frequency"

For a given medium where $\beta(\omega)$ is known, one can compute the value of β_2 near a given carrier frequency, ω_0 , as

$$\beta_2(\omega) = \beta_2|_{\omega=\omega_0} + \beta_3|_{\omega=\omega_0} \cdot (\omega - \omega_0) + \frac{1}{2}\beta_4|_{\omega=\omega_0} \cdot (\omega - \omega_0)^2 + \dots, \quad (4.14)$$

which allows one to solve for the specific frequency (or *frequencies*, plural!), ω_{ZD} , where $\beta_2(\omega_{ZD}) = 0$. This "Zero Dispersion Frequency" is important because a number of nonlinear mechanisms are more efficient for frequencies at ω_{ZD} or ones close to it where $\beta_2 < 0$. Therefore, determining the value(s) of ω_{ZD} for a given medium is crucial when conducting experiments in nonlinear optics. The zero dispersion frequency of a particular fiber can be measured experimentally using commonly available optical laboratory equipment [13]. Historically, optical fibers for telecommunication were designed so that $\beta_2 \approx 0$ close to near-infrared frequencies of laser light (≈ 190 - 230 THz ≈ 1310 - 1550 nm) that were easy to generate, modulate and detect. The intention was to prevent temporal broadening and thus overlap and interference of pulses carrying digital information. Since the mid 2000's, advancements in electronic dispersion compensation have rendered such fiber designs obsolete and even deleterious, as nonlinear effects that distort signals by altering their phases and amplitudes are more significant close to ω_{ZD} .

4.5 β_n - Higher order delays

Having understood that the slope of $\beta(\omega)$ (i.e. β_1) determines the propagation speed of the pulse envelope while the curvature of $\beta(\omega)$ (i.e. β_2) determines the temporal broadening of the pulse, these insights can be generalized. For example, $\beta_3 > 0$ implies that the term $i\beta_3/6(\omega - \omega_0)^3 z$ causes a positive $\partial_\omega \phi$ for all frequencies except the carrier. Thus, both the higher and lower frequencies contributing to the pulse will begin to trail behind the main pulse, leading to asymmetric temporal broadening. Furthermore, $\beta_4 > 0$ implies that $i\beta_4/24(\omega - \omega_0)^4 z$ causes additional symmetric temporal broadening on top of what is caused by β_2 . See Fig. 4.2 for an illustration of the impact of different β_n terms on the temporal profile of a Gaussian pulse. How many terms in the expansion of $\beta(\omega)$ to include when analyzing the evolution of a pulse propagating through a medium depends on the spectral width of the pulse, which is inversely proportional to its duration. For pulses above 1 ps, orders higher than β_3 rarely contribute much. In numerical simulations of supercontinuum generation with pulses with a duration on the scale of 10 fs, orders up to β_8 are often included

for good measure. Similarly to Eq. 4.13, the characteristic lengths over which higher order dispersion effects become significant are defined by

$$L_n = \frac{T_0^n}{|\beta_n|}. \quad (4.15)$$

See [this video tutorial](#) for further details on dispersion.

4.6 Are $\alpha(\omega)$ and $\beta(\omega)$ independent?

In Eq. 1.1, α is treated as a constant because its frequency dependence is usually weak across the bandwidth of a typical pulse. However, one could in principle include a Taylor expansion of $\alpha(\omega)$ as was done with $\beta(\omega)$. Interestingly, it turns out that the functions $\alpha(\omega)$ and $\beta(\omega)$ for a given medium are related through the so-called [Kramers-Kronig Relations](#) and that knowing one enables the calculation of the other. As a consequence, $\alpha(\omega)$ and $\beta(\omega)$ *cannot* be chosen independently. Proving the connection mathematically is tricky, but physically, the intuition is that the frequency dependent absorption of $\alpha(\omega)$ fundamentally is exactly what gives rise to frequency dependent phase delay, $\beta(\omega)$. Additionally, the response of the medium at a given location to an applied electric field can only depend on *the current and past* values of the electric field at that location for causality to be respected, which further constrains what combinations of attenuation and phase delay are allowed. Conveniently, it turns out that if $\alpha(\omega) = \alpha$ is treated as a constant w.r.t. frequency, its value can be changed freely without impacting any of the values of β_n .

Please see [this video](#) and [this other video](#) for more details on the Kramers-Kronig Relations. See [this interactive graph](#) for a tutorial on using causality and the Kramers-Kronig Relations in the time domain to relate $\alpha(\omega)$ to $\beta(\omega)$.

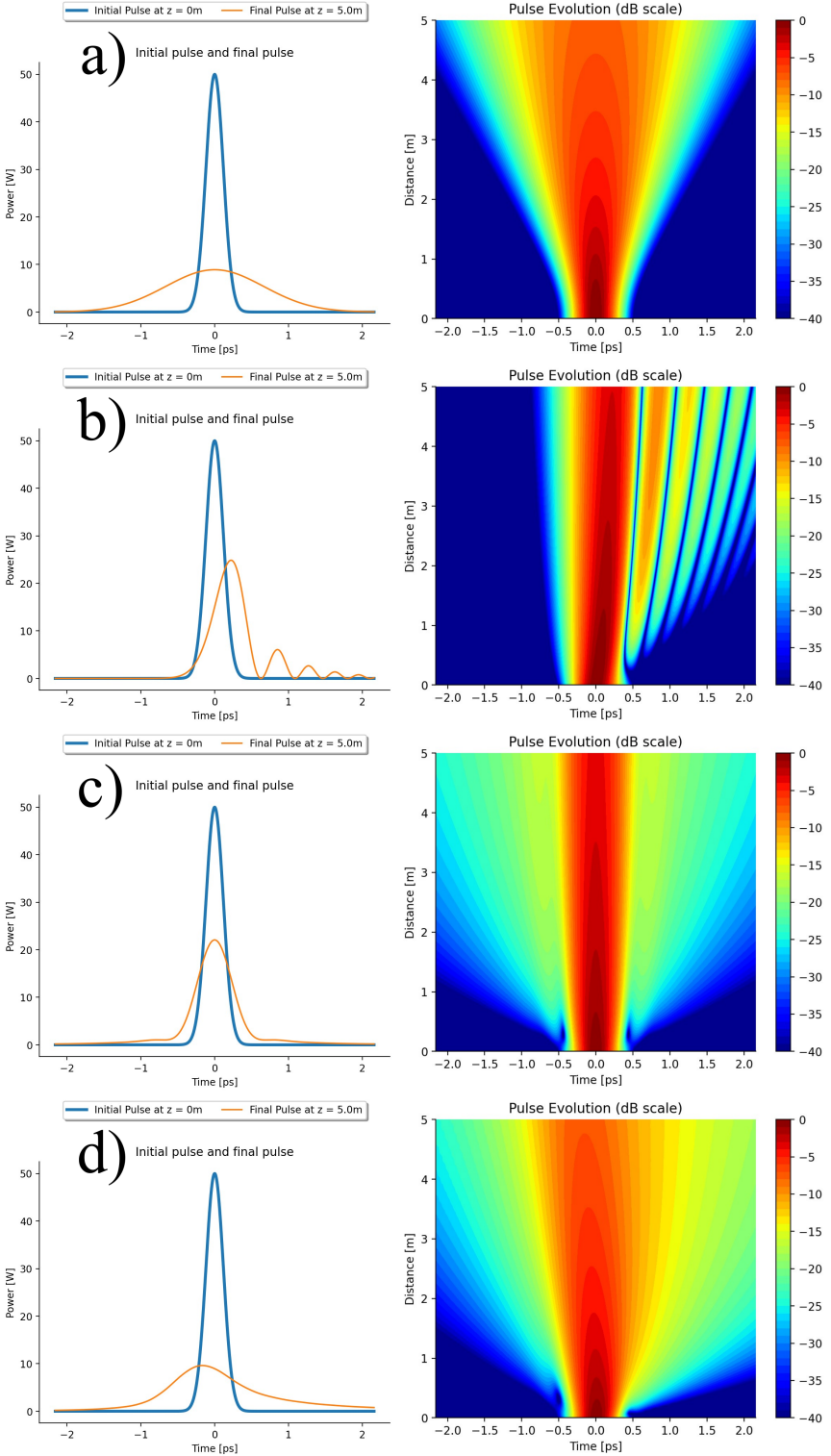


Figure 4.2: Illustration of the effect of different β_n terms on a Gaussian pulse in the time domain. Left column shows a comparison of the power envelope of the pulse before and after propagating through media with different β_n terms. Right column shows the evolution of the power envelope with distance. a) Medium with $\beta_2 < 0$. b) Medium with $\beta_3 > 0$. c) Medium with $\beta_4 < 0$. d) Medium where $\beta_2 < 0$, $\beta_3 > 0$ and $\beta_4 < 0$ are present simultaneously. Figures generated using the numerical simulation in [this interactive notebook](#), which the reader is encouraged to experiment with.

Chapter 5

Self Phase Modulation

In materials with a third order nonlinearity, the refractive index at some instant depends on the optical power at that instant. Thus, a high power pulse will experience a greater change in its phase than an equivalently shaped pulse with lower power. Because many different frequencies of light can be present in a nonlinear medium at the same time, describing the impact of the nonlinearity on the optical field can be complicated. This chapter explains the simple case, labelled "Self Phase Modulation" (SPM), where only a single pulse centered at a single carrier frequency is present.

5.1 Phase change across pulse

Starting from Eq. 1.1 and assuming that all parameters except $\gamma > 0$ are zero, that $\omega_0 \mathbf{A} \gg \partial_T \mathbf{A}$ and that $R(T_{\text{delay}}) = \delta(T_{\text{delay}})$, the Generalized Nonlinear Schrödinger Equation reduces to

$$\partial_z \mathbf{A} = i\gamma |\mathbf{A}|^2 \mathbf{A}. \quad (5.1)$$

Mathematically, Eq. 5.1 states that for a small change in z , the complex number, \mathbf{A} , changes by an amount that is equal to itself rotated 90 degrees in the complex plane ($i\mathbf{A}$) and scaled by its own squared magnitude ($|\mathbf{A}|^2$) as well as a scalar, γ . Physically, Eq. 5.1 implies that the nonlinearity alters the instantaneous phase of the field by an amount that depends on its power, but does not alter the magnitude of the power at that instant. Solving Eq. 5.1 yields

$$\mathbf{A}(z, T) = \mathbf{A}(0, T) \exp(i\gamma |\mathbf{A}(0, T)|^2 z). \quad (5.2)$$

To understand the implications of Eq. 5.2, consider Eq. 2.11, which states that the instantaneous frequency of a pulse is related to the negative derivative of its phase

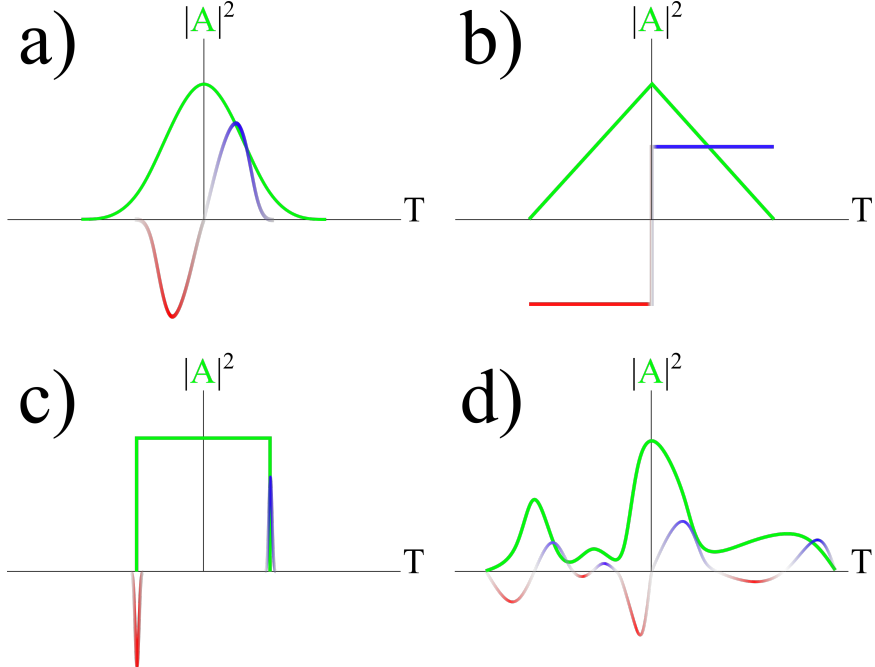


Figure 5.1: Visualization of the impact of SPM on a) a Gaussian pulse, b) a triangular pulse, c) a square pulse, d) an arbitrary pulse. In general, positive slopes result in a red-chirp, decreasing slope leads to a blue-chirp and horizontal slopes result in no chirp.

w.r.t. time. Assuming a Gaussian pulse so that $A(0, T) = A_0 \exp(-T^2/2T_0^2)$, the instantaneous frequency of this pulse after passing a distance, z , through a nonlinear medium is

$$\begin{aligned} \delta\omega(z, T) &= -\gamma |A_0|^2 z \partial_T \exp\left(-\frac{T^2}{T_0^2}\right) \\ &= 2\gamma |A_0|^2 z T / T_0^2 \exp\left(-\frac{T^2}{T_0^2}\right), \end{aligned} \quad (5.3)$$

which implies that the pulse will develop a red-chirp in the front and a blue-chirp in the back. See Fig. 5.1(a) for a visualization of the chirp generated by a Gaussian pulse and Fig. 5.1(b-d) for visualizations of the chirps generated by other pulse profiles. Considering the argument of the exponential in Eq. 5.2, a characteristic length over which nonlinear effects become significant can be defined as

$$L_{NL} = \frac{1}{\gamma P_0} = \frac{1}{\gamma |A(0, T)|^2}, \quad (5.4)$$

where P_0 is the initial peak power of the pulse.

5.2 Spectral broadening

The analysis of Eq. 5.3 showed that SPM causes pulses to become "more red" at leading slopes and "more blue" at trailing slopes. Considered in isolation, $\beta_2 > 0$ would result in a similar behavior, but the key difference is that dispersion only changes the relative phase of different frequency components, while SPM also alters their magnitudes. In other words, SPM applied to a pulse generates new colors, which were not present initially! That Eq. 5.1 implies broadening in the spectral domain can be seen mathematically by taking the Fourier Transform on both sides of the equality and recalling that the Fourier Transform of a product of two functions in the time domain is equivalent to the convolution in their spectra in the frequency domain:

$$\begin{aligned}\partial_z \tilde{\mathbf{A}} &= i\gamma \mathfrak{F} \{ \mathbf{A} \mathbf{A}^* \mathbf{A} \} \\ &= i\gamma \tilde{\mathbf{A}} * \tilde{\mathbf{A}}^* * \tilde{\mathbf{A}}.\end{aligned}\tag{5.5}$$

In short, Eq. 5.5 implies that the change in the spectrum of \mathbf{A} w.r.t. z depends on the convolution of that spectrum with itself and its complex conjugate. Since convolving two functions yields a new function broader than the initial ones, Eq. 5.5 shows that the spectrum will tend to broaden with distance, implying that new frequencies are added by transferring power from the carrier towards the red and blue ends. See Fig. 5.2 for an illustration of the impact of SPM on a Gaussian pulse.

5.3 SPM, Attenuation and "Effective Length"

Consider Eq. 1.1 with the same assumptions as for Eq. 5.1, but where additionally $\alpha \neq 0$. Recall also from Eq. 3.2 that $\alpha \neq 0$ causes the power of the pulse to change exponentially with distance. In this case,

$$\begin{aligned}\partial_z \mathbf{A} &= \frac{\alpha}{2} \mathbf{A} + i\gamma |\mathbf{A}|^2 \mathbf{A} \\ &= \left(\frac{\alpha}{2} + i\gamma |\mathbf{A}(0, T)|^2 \exp(\alpha z) \right) \mathbf{A}.\end{aligned}\tag{5.6}$$

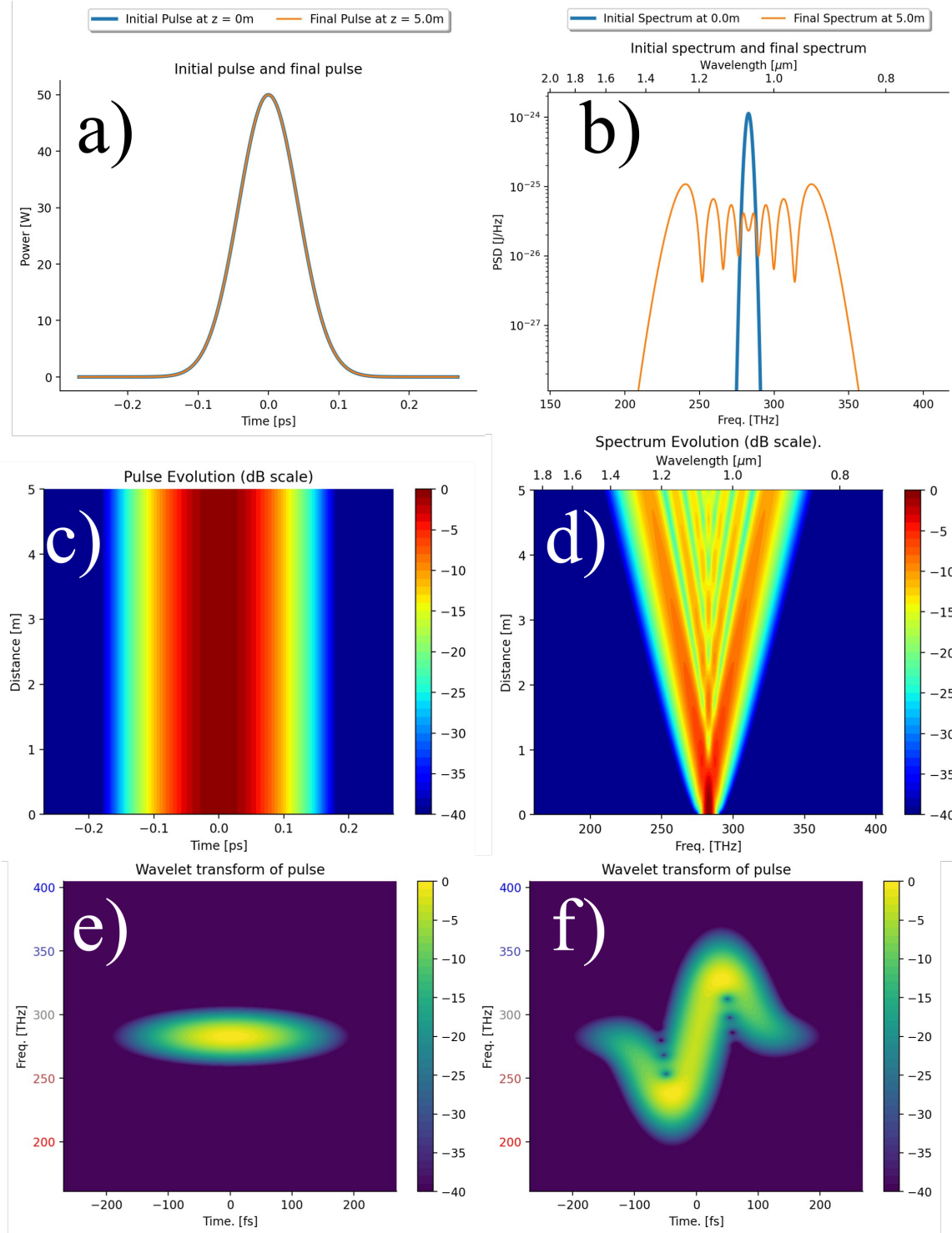


Figure 5.2: Before-and-after comparison of a Gaussian pulse propagating through a nonlinear medium described by Eq. 5.1. a) In the time domain, the power envelope of the pulse is unchanged. b) The spectrum broadens. c) Evolution of the power envelope in the time domain exhibits no change. d) The spectrum gradually broadens. e) Spectrogram of pulse before propagation. f) Spectrogram of pulse after propagation. Note the broadening in the spectral domain and constant width in the temporal domain. Figures generated using the numerical simulation in [this interactive notebook](#), which the reader is encouraged to experiment with.

Integrating Eq. 5.6 from 0 to z yields

$$\begin{aligned}\mathbf{A}(z, T) &= \mathbf{A}(0, T) \exp\left(\frac{\alpha}{2}z + i\gamma|\mathbf{A}(0, T)|^2 \int_0^z \exp(\alpha\xi) d\xi\right) \\ &= \mathbf{A}(0, T) \exp\left(\frac{\alpha}{2}z + i\gamma|\mathbf{A}(0, T)|^2 \frac{\exp(\alpha z) - 1}{\alpha}\right) \\ \mathbf{A}(L, T) &= \mathbf{A}(0, T) \exp\left(\frac{\alpha}{2}z + i\gamma|\mathbf{A}(0, T)|^2 L_{eff}\right),\end{aligned}\quad (5.7)$$

where the "Effective Length" of the medium with an actual length of L is defined as

$$L_{eff} = \frac{\exp(\alpha L) - 1}{\alpha}. \quad (5.8)$$

The insight provided by Eq. 5.7 and Eq. 5.8 is that while nonlinear effects generally become more pronounced by letting the light propagate through a longer medium, the attenuation of that medium will eventually decrease the optical power to a point where all nonlinear effects become negligible. For example, the effective length of a typical 100 km single-mode fiber for telecommunications, which has a loss coefficient of $\alpha = -0.22\text{dB/km}$ is approximately 19.6 km. In other words, an optical signal would accumulate approximately the same nonlinear phase shift propagating through the 100 km lossy fiber as it would have accumulated by propagating through a lossless one with a length of only 19.6km. See [this interactive graph](#) for an illustration of how the effective length depends on α . Note that $L_{eff} \approx L$ when $\alpha L \ll 1$ and that $L_{eff} > L$ is possible when $\alpha > 0$, which is the case in optical amplifiers. Furthermore, α may depend on z in special non-uniform fibers or ones where Raman amplification is present, in which case Eq. 3.1 and thus Eq. 5.6 should be changed accordingly.

5.4 Self-Steepening

In Eq. 5.1, it is assumed that the nonlinear phase shift is proportional to the field enveloped multiplied by its average power, $\mathbf{A}|\mathbf{A}|^2$. This assumption can be viewed as a zeroth-order Taylor-approximation w.r.t. time of the nonlinear response, in the same way that one can approximate $\exp(x) \approx 1$ for very small values of x . Assuming instead that the rate of change in the field envelope multiplied by its average power, $\partial_T(\mathbf{A}|\mathbf{A}|^2)$, also contributes yields

$$\partial_z \mathbf{A} = i\gamma \left(1 + \frac{i}{\omega_0} \partial_T\right) \mathbf{A}|\mathbf{A}|^2. \quad (5.9)$$

The first term in the parenthesis in Eq. 5.9 is SPM, while the second term is referred to as "self-steepening" (SS). Physically, this can be understood by considering that the nonlinearity causes a large change in the refractive index where the pulse power is high. A higher refractive index implies slower light propagation, causing the peak of a high power pulse to slow down relative to less intense parts as it propagates forward, thereby causing a build-up of power at later times and thus a steep, decreasing slope. Analogously, a large, unaerodynamic truck suddenly experiencing strong head-wind will slow down a lot compared to more streamlined cars and thereby cause a jam behind it, while traffic becomes less dense in front. Since SS flattens the power slope in front of the pulse and steepens it in the back, it preferentially blue-shifts the spectrum of the pulse, since $\delta\omega \propto -\partial_T|A|^2$. See Fig. 5.3 for an illustration of the impact of SS on the same Gaussian pulse as in Fig. 5.2. For a Gaussian pulse subjected only to SPM and self-steepening, **it can be shown** that its back slope becomes infinitely steep at a distance of

$$L_{SS} = \frac{T_0\omega_0 \exp(1/2)}{3\sqrt{2}\gamma P_0}. \quad (5.10)$$

See [this video tutorial](#) for more information on SS.

5.4.1 Applicability

Since the impact of SS is inversely proportional to $\omega_0 \approx 2\pi/200 \text{ THz} = 2\pi/5\text{fs}$ and the time derivative of $A|A|^2$ is small for long pulses, SS is significant for pulse durations below 100 fs, somewhat significant for pulse durations on the scale of 100s of fs and negligible for pulse durations longer than a few ps.

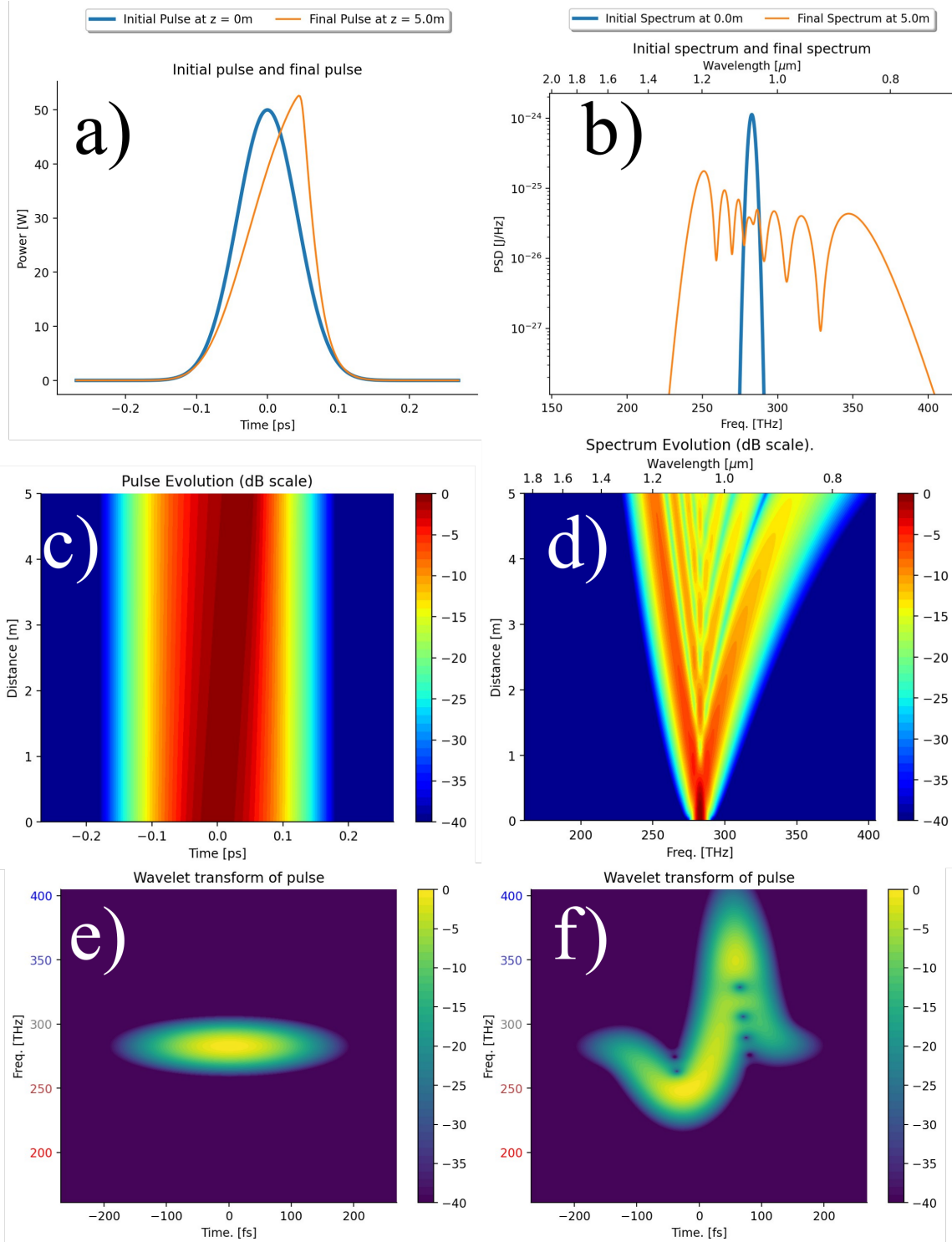


Figure 5.3: Before-and-after comparison of a Gaussian pulse propagating through a nonlinear medium described by Eq. 5.9. a) In the time domain, the power envelope of the pulse becomes steeper in the back because the peak of the pulse experiences a higher refractive index due to the nonlinearity and slows down. b) The spectrum broadens asymmetrically towards higher frequencies due to the steep, decreasing slope in the back. c) Evolution of the power envelope in the time domain. d) The spectrum gradually broadens towards higher frequencies. e) Spectrogram of pulse before propagation. f) Spectrogram of pulse after propagation. Figures generated using the numerical simulation in [this interactive notebook](#), which the reader is encouraged to experiment with.

Chapter 6

Four Wave Mixing

The average power of a single frequency of light calculated from Eq. 2.5 will be constant over time. If two frequencies are present, their interference will cause the average power to vary sinusoidally over time. Since $\gamma \neq 0$ implies that the refractive index depends on power, the simultaneous presence of two frequencies of light in a nonlinear medium implies that the phase will be sinusoidally modulated. This effect generates new frequency components and is referred to as "Four Wave Mixing" (FWM).

6.1 Electrical phase modulation

To understand FWM, first consider a continuous wave laser signal launched into a commercially available phase modulator being driven by an sinusoidal electrical signal from a function generator. See Fig. 6.1 for a visualization and [this video](#) for an experimental demonstration. The signal at the output is given by

$$\mathbf{E}_{out} = \mathbf{E}_{in} \exp(i\Phi \cos(\omega_d T),) \quad (6.1)$$

where Φ is the maximum phase shift imparted by the modulator and ω_d is the modulation frequency. See [this interactive graph](#) for an illustration of the impact of this modulation on the real part of \mathbf{E}_{out} . Using the so-called "Jacobi-Anger Expansion" [14], the cosine function inside the complex exponential in Eq. 6.1 can be written as

$$\exp(i\Phi \cos(\omega_d T)) = \sum_{n=-\infty}^{\infty} i^n J_n(\Phi) \exp(in\omega_d T), \quad (6.2)$$

where $J_n(\Phi)$ is the n^{th} order Bessel function of the 1st kind. In short, Eq. 6.2 shows that sinusoidal phase modulation gives rise to new discrete frequency components spaced ω_d apart and whose relative powers depend on the modulation amplitude, Φ . Note also that applying Eq. 2.11 to Eq. 6.1 shows that the sinusoidal modulation changes the instantaneous frequency over time by $\Phi\omega_d \sin(\omega_d T)$, further suggesting that phase modulation changes the color of the incident light.

6.2 Nonlinearity based phase modulation

The following approach to modelling FWM is inspired by the one originally presented in [15]. Consider Eq. 5.2 and assume that the field, $\mathbf{A}(0, T)$ can be written as the sum of two continuous wave signals with average powers P_a and P_b and a frequency spacing of $\Delta\omega$ according to

$$\mathbf{A}(0, T) = \sqrt{P_a}e^{-i\frac{\Delta\omega}{2}T} + \sqrt{P_b}e^{i\frac{\Delta\omega}{2}T}. \quad (6.3)$$

When the signal consists of two pulses with finite durations, the continuous wave assumption is an approximation, which is valid when ω_d is larger than the bandwidths of the pulses. The field at the end of the nonlinear medium is

$$\begin{aligned} \mathbf{A}(L, T) &= \mathbf{A}(0, T) \exp\left(i\gamma L[P_a + P_b + 2\sqrt{P_a P_b} \cos(\omega_d T)]\right) \\ &= \mathbf{A}(0, T) \exp(i\gamma L[P_a + P_b]) \exp\left(i2\gamma L\sqrt{P_a P_b} \cos(\omega_d T)\right) \\ \mathbf{A}(L, T)Q^{-1} &= \mathbf{A}(0, T) \exp\left(i2\gamma L\sqrt{P_a P_b} \cos(\omega_d T)\right) \\ \mathbf{A}(L, T)Q^{-1} &= \mathbf{A}(0, T) \exp(i\phi_{NL} \cos(\omega_d T)), \end{aligned} \quad (6.4)$$

where the time-independent factor $Q = \exp(i\gamma L[P_a + P_b])$ is temporarily moved to the left hand side of the equality for convenience. Applying Eq. 6.2 yields

$$\begin{aligned} \mathbf{A}(L, T)Q^{-1} &= \mathbf{A}(0, T) \sum_{n=-\infty}^{\infty} i^n J_n(\phi_{NL}) e^{in\omega_d T} \\ &= \left(\sqrt{P_a}e^{-i\frac{\Delta\omega}{2}T} + \sqrt{P_b}e^{i\frac{\Delta\omega}{2}T}\right) \sum_{n=-\infty}^{\infty} i^n J_n(\phi_{NL}) e^{in\omega_d T} \\ &= \sqrt{P_a} \sum_{m=-\infty}^{\infty} i^m J_m(\phi_{NL}) e^{i(m-\frac{1}{2})\omega_d T} + \dots \\ &\quad \sqrt{P_b} \sum_{k=-\infty}^{\infty} i^k J_k(\phi_{NL}) e^{i(k+\frac{1}{2})\omega_d T}. \end{aligned} \quad (6.5)$$

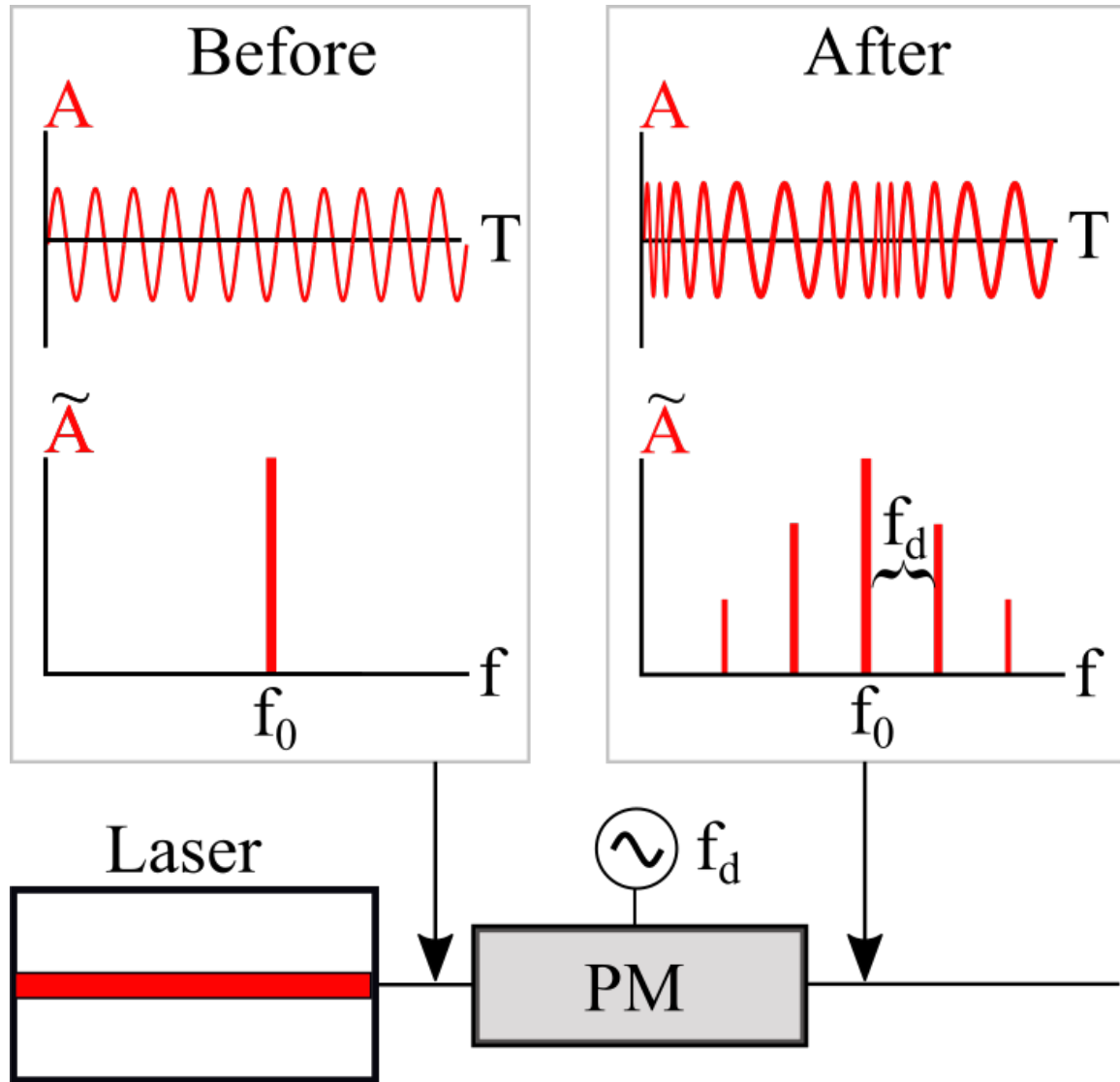


Figure 6.1: Illustration of the impact of electrical sinusoidal phase modulation of a continuous wave optical signal. Before entering the modulator, only a single laser frequency is present. After the modulator, the alternating advancement and delay of the optical phase in the time domain is equivalent to introducing new frequency components according to Eq. 6.2.

Note that the infinite sum initially indexed by n is split into two infinite sums indexed by m and k because the two complex exponentials in $\textcolor{red}{A}(0, T)$ cause the frequency corresponding to $m = 1$ in the first sum to be different from the one corresponding to $k = 1$ in the second sum. To re-combine the two sums, use $m = k + 1$ and obtain

$$\begin{aligned}\textcolor{red}{A}(L, T)Q^{-1} &= \sqrt{P_a} \sum_{k=-\infty}^{\infty} i^{k+1} J_{k+1}(\phi_{NL}) e^{i(k+\frac{1}{2})\omega_d T} + \dots \\ &\quad \sqrt{P_b} \sum_{k=-\infty}^{\infty} i^k J_k(\phi_{NL}) e^{i(k+\frac{1}{2})\omega_d T} \\ &= \sum_{n=-\infty}^{\infty} i^n \left[i\sqrt{P_a} J_{n+1}(\phi_{NL}) + \sqrt{P_b} J_n(\phi_{NL}) \right] e^{i\omega_d(n+\frac{1}{2})T}.\end{aligned}\tag{6.6}$$

Finally, moving Q to the right hand side of Eq. 6.6 yields

$$\textcolor{red}{A}(L, T) = \sum_{n=-\infty}^{\infty} i^n \left[i\sqrt{P_a} J_{n+1} \left(2\gamma L \sqrt{P_a P_b} \right) + \sqrt{P_b} J_n \left(2\gamma L \sqrt{P_a P_b} \right) \right] e^{i\omega_d(n+\frac{1}{2})T + i\gamma L[P_a + P_b]}.\tag{6.7}$$

In Eq. 6.7, the frequency component for which $n = -1$ will be at $-\omega_d/2$, while the one for which $n = 0$ will be at $+\omega_d/2$, corresponding to the original two frequencies in Eq. 6.3. The average power of the n^{th} order sideband is

$$|\textcolor{red}{A}_n(L, T)|^2 = P_a J_{n+1}^2 \left(2\gamma L \sqrt{P_a P_b} \right) + P_b J_n^2 \left(2\gamma L \sqrt{P_a P_b} \right).\tag{6.8}$$

See Fig. 6.2 a) and b) for a numerical simulation of the sideband powers for different values of $2\gamma L \sqrt{P_a P_b}$. See Fig. 6.2 c) for a comparison of the numerically calculated sideband powers and the ones predicted by Eq. 6.8. Assuming that $P_a \ll P_b$ and $2\gamma L \sqrt{P_a P_b} < \sqrt{1+n}$ with $n > 0$ yields

$$|\textcolor{red}{A}_n(L, T)|^2 \approx P_b \frac{(\gamma^2 L^2 P_a P_b)^n}{n!^2},\tag{6.9}$$

since

$$J_n(x) \approx \frac{1}{n!} \left(\frac{x}{2} \right)^n\tag{6.10}$$

for small arguments in the Bessel function. See Fig. 6.2 d) for an illustration of the scaling behavior predicted by Eq. 6.9. The fact that the power of higher order sidebands is more sensitive to changes in input power than lower order ones is useful for various all-optical signal processing techniques [16, 17, 18]. See [this tutorial video](#)

for a different approach to modelling FWM that takes dispersion into account. See [this video](#) for an experimental demonstration of FWM.

6.3 Cross Phase Modulation (XPM)

In Chapter 5, it was shown that the phase of a single-frequency optical field in a nonlinear medium increases linearly with the average power of that field. When two frequencies are present, the phase of one frequency component as a function of its own average power and the average power of the other can be calculated from Eq. 6.7. Choosing the $n = 0$ component yields

$$\phi_0 = \frac{\omega_d}{2}T + \gamma L[P_a + P_b] + \theta_0, \quad (6.11)$$

where

$$\begin{aligned} \theta_0 &= \arg \left(i\sqrt{P_a}J_1 \left(2\gamma L\sqrt{P_a P_b} \right) + \sqrt{P_b}J_0 \left(2\gamma L\sqrt{P_a P_b} \right) \right) \\ &= \arctan \left(\frac{\sqrt{P_a}J_1 \left(2\gamma L\sqrt{P_a P_b} \right)}{\sqrt{P_b}J_0 \left(2\gamma L\sqrt{P_a P_b} \right)} \right). \end{aligned} \quad (6.12)$$

Using Eq 6.10 allows Eq. 6.12 to be written as

$$\begin{aligned} \theta_0 &\approx \arctan \left(\frac{\sqrt{P_a}\gamma L\sqrt{P_a P_b}}{\sqrt{P_b}} \right) \\ &\approx \arctan (\gamma L P_a) \\ &\approx \gamma L P_a. \end{aligned} \quad (6.13)$$

Thus, the phase of the $n = 0$ frequency component is

$$\begin{aligned} \phi_0 &\approx \frac{\omega_d}{2}T + \gamma L[P_a + P_b] + \gamma L P_a \\ &= \frac{\omega_d}{2}T + \gamma L[2P_a + P_b]. \end{aligned} \quad (6.14)$$

Note that $n = 0$ is the frequency at $+\omega_d/2$, which initially had the average power P_b . Therefore, the term in Eq. 6.14 containing P_b corresponds to the impact of SPM, while the term containing P_a corresponds to so-called "Cross Phase Modulation" (XPM). Interestingly, Eq. 6.14 shows that XPM is "twice as strong" as SPM as demonstrated numerically in Fig. 6.3. See [this video tutorial](#) for an alternative derivation starting from Maxwell's Equations of the impact of XPM. See [this interactive graph](#) for an illustration of the relative impact of SPM and XPM on two waves with different frequencies.

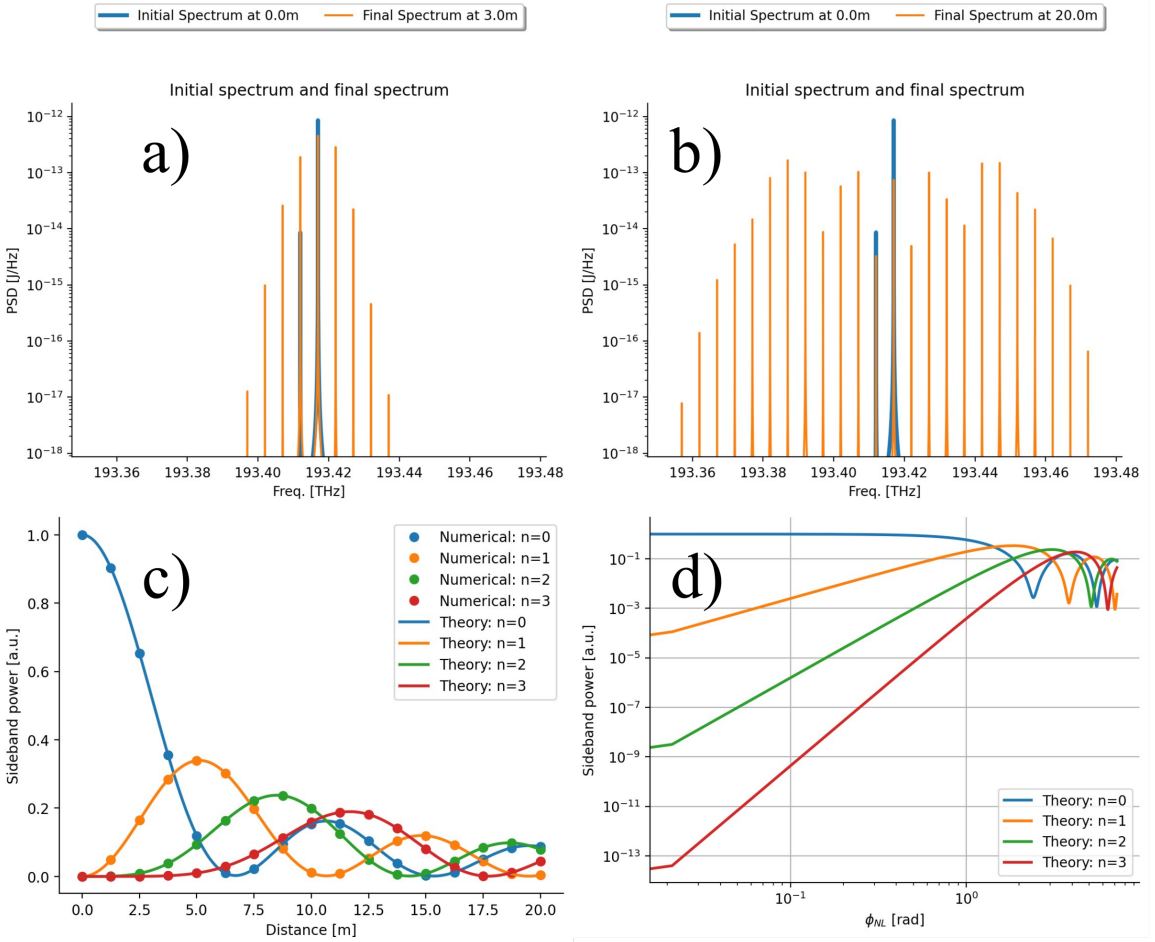


Figure 6.2: a) Numerically calculated initial and final spectrum when two frequencies with $P_b = 100P_a$ spaced 5 GHz apart propagate through a medium where $\phi_{NL} = 2\gamma L \sqrt{P_a P_b} = 1.08$ rad. Note the transfer of power from the most intense frequency into neighbouring sidebands and the rapid decrease in power for increasing sideband orders as predicted by Eq. 6.9. b) Same as a) but for $\phi_{NL} = 2\gamma L \sqrt{P_a P_b} = 7.2$ rad. c) Comparison of sideband power normalized to P_b according to numerical simulations and Eq. 6.8. d) Similar to c) but plotted on a double-log scale versus ϕ_{NL} to demonstrate the scaling behavior predicted by Eq. 6.9. Figures generated using [this interactive notebook](#), which the reader is encouraged to experiment with.

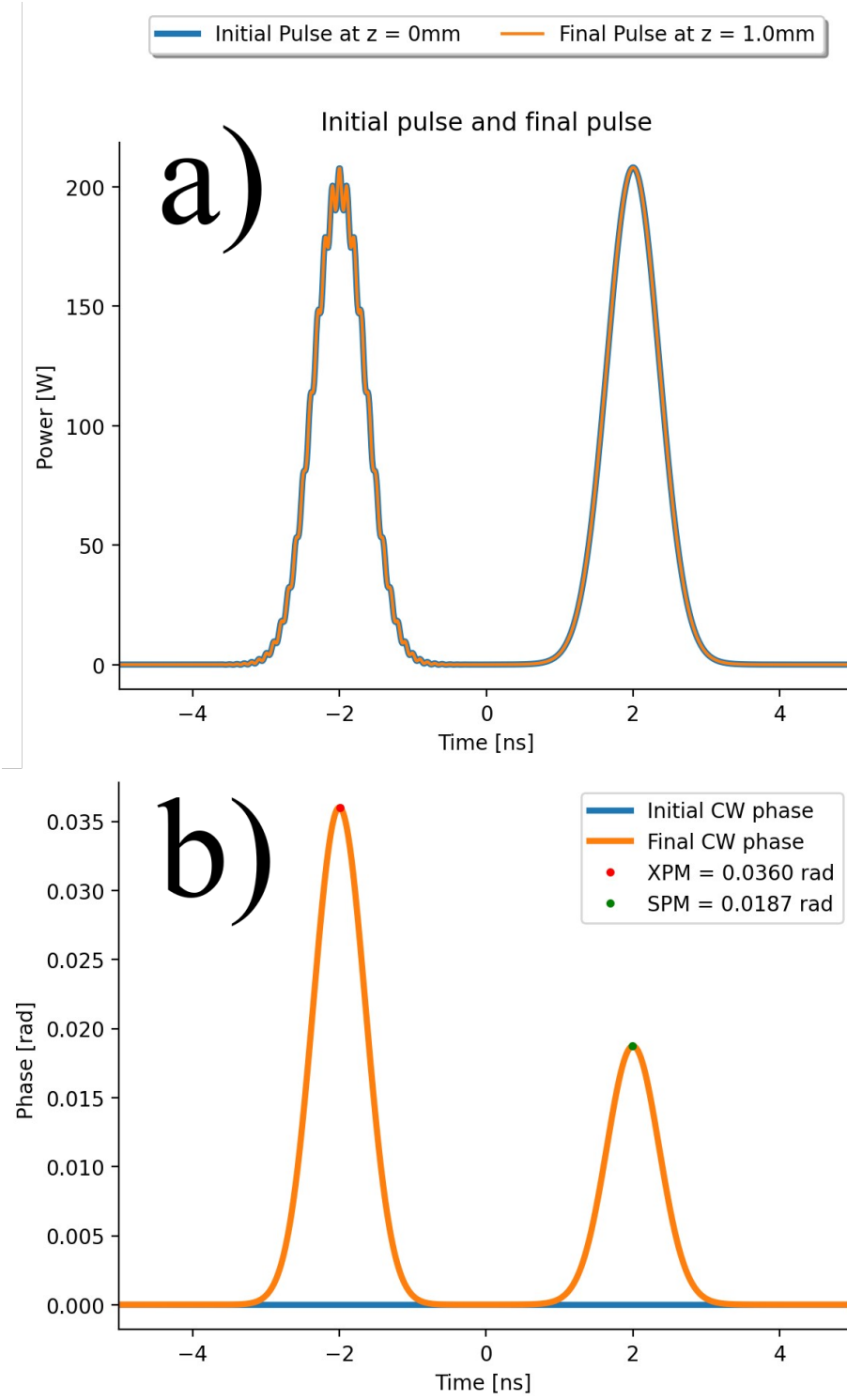


Figure 6.3: Illustration of the disparate impacts of SPM and XPM on the phase of an optical signal. a) Time domain representation of a low power CW signal overlapped with two identical, high power Gaussian pulses that only differ by their carrier frequencies. The carrier frequency of the pulse on the left is 10 GHz below the carrier frequency of the CW light. b) After simulating the propagation through a nonlinear medium, the CW light obtains approximately twice the phase shift from XPM as from SPM as predicted by Eq. 6.14. The ratio of $0.0360/0.0187 \approx 1.925 \neq 2$ is attributed to the approximations involved in Eq. 6.14 and to the finite time resolution of the simulation. Figures generated using [this interactive notebook](#), which the reader is encouraged to experiment with.

6.4 Phase matching

The derivation presented in Section 6.2 assumes negligible dispersion, which is the case for a small ω_d value and a carrier frequency close to the zero dispersion frequency explained in Subsection 4.4.1. The impact of dispersion on FWM is explained in [this video tutorial](#). It turns out that FWM is weak for positive values of β_2 and is most significant when

$$0 = \beta_2 \omega_d^2 + \gamma(P_a + P_b) \quad (6.15)$$
$$\beta_2 = -\gamma(P_a + P_b)/\omega_d^2 < 0,$$

assuming that ω_d is small enough for β_2 to be the only relevant term in Eq. 4.2. The reason is that FWM as a process involves the *coherent* transfer of power from one set of electromagnetic waves into oscillating changes in the refractive index of the nonlinear medium and then into another set of electromagnetic frequencies. In short, the nonlinearity ensures that the incident electromagnetic waves will cause the tiny dipoles constituting the medium to oscillate at new temporal frequencies. If the corresponding spatial frequency of one of these temporal oscillations in the dipoles is the same as the spatial frequency of another electromagnetic wave, its power will increase with distance via constructive interference as explained in [this video tutorial](#). The requirement in Eq. 6.15 arises because the difference in spatial frequencies of the incident waves and the new wave should be small and because the increase in the refractive index due to the power of the initial fields makes the spatial frequencies larger than they normally would be. Thus, a negative values of β_2 is needed to compensate. This effect, where the spatial frequencies caused by the regular refractive index of the medium balance changes in the spatial frequencies due field power via nonlinearity, is referred to as "phase matching". The phase matching condition in Eq. 6.15 is relevant for the special case of FWM and similar expressions can be derived for other nonlinear effects beyond the scope of this primer, such as [Second-Harmonic generation](#), [Third-Harmonic generation](#) and [Stimulated Brillouin Scattering](#).

6.4.1 Modulation Instability

As a consequence of FWM, a signal with a carrier frequency where $\beta_2 < 0$ for a particular nonlinear medium will get noisier as it propagates forward. The reason is that the interference between the carrier and tiny, ubiquitous fluctuations in the electromagnetic field will cause FWM to transfer optical power away from the carrier

and into adjacent frequencies as explained [here](#) and illustrated in Fig. 6.4. The process of particular noise frequencies being preferentially amplified due to phase matching is referred to as "Modulation Instability" (MI). See [this video tutorial](#) for further details on MI.

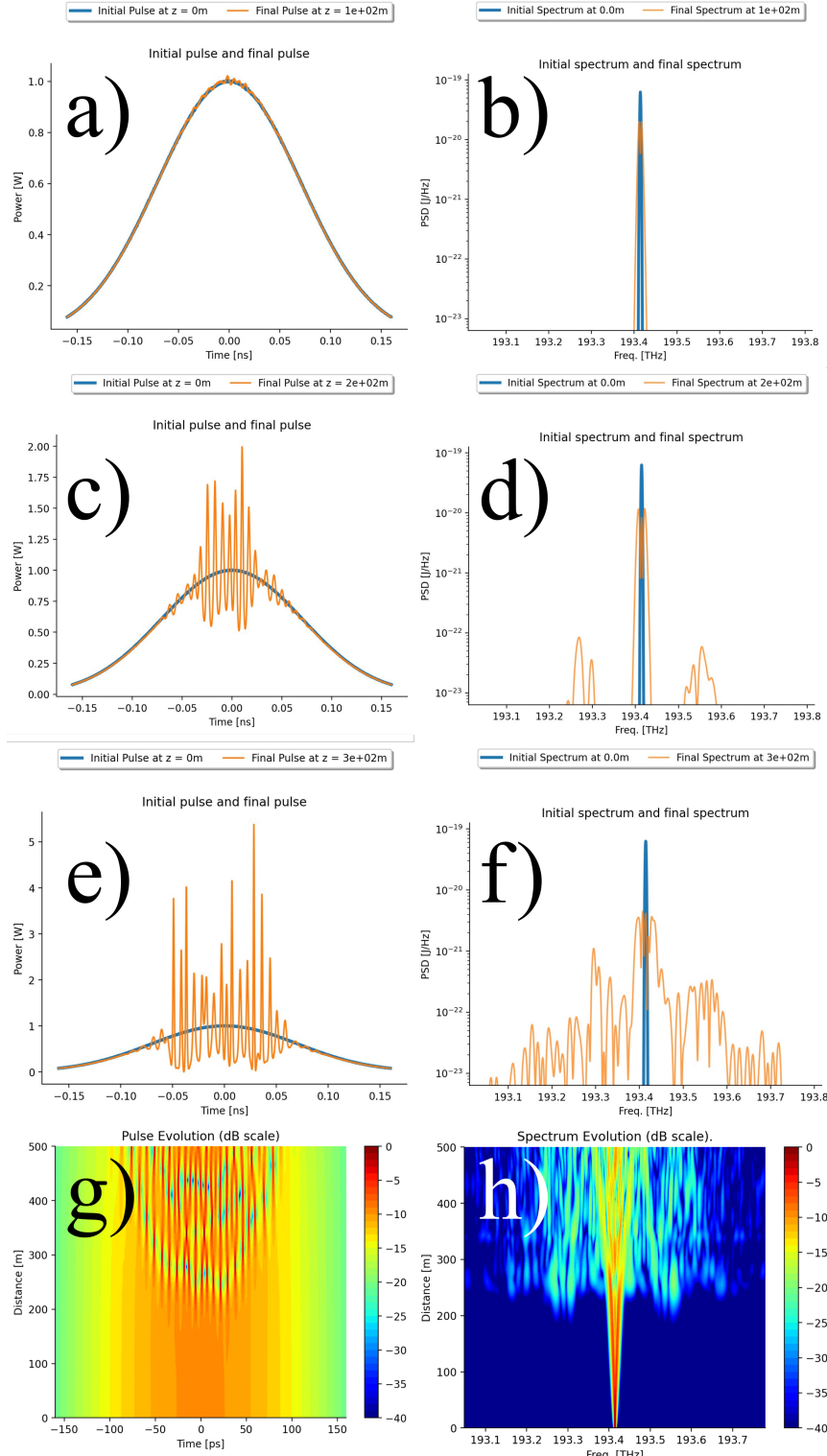


Figure 6.4: a) Initial and final time domain power of a signal consisting of a Gaussian pulse and random noise with an amplitude 1.000 times smaller than that of the Gaussian propagated through 100m of a nonlinear medium with $\beta_2 < 0$. b) Same as a) but showing the spectrum. c-d) Same as a-b) but for a distance of 200m. e-f) Same as a-b) but for a distance of 300m. g) full temporal evolution for 500m. h) Same as g) but for the spectrum. Figures generated using [this interactive notebook](#), which the reader is encouraged to experiment with.

Chapter 7

The Raman effect

When exposed to an oscillating electromagnetic field, the electrons in the medium will respond almost instantly due to their low mass. The nuclei around which these electrons orbit will react much more slowly due to their comparatively large mass. The result is that the nonlinear phase shift affecting a particular instant of a pulse for a certain fiber segment depends on two things: The optical power of the pulse at that instant and the optical power that affected that location in the past. The nonlinear impact that time-delayed mechanical vibrations of the nuclei in the material lattice have on the electromagnetic field that induced them is called the "Raman effect" [19].

7.1 The Raman response function

Mathematically, the impact of the Raman effect on an optical pulse can be described by

$$\partial_z \mathbf{A} = i\gamma \left(\mathbf{A} \int_0^\infty R(T_{delay}) |\mathbf{A}(z, T - T_{delay})|^2 dT_{delay} \right), \quad (7.1)$$

which is equivalent to Eq. 1.1 when attenuation, dispersion and self-steepening are ignored. The function, $R(T_{delay})$ is the total response function, which indicates how much the power at different times in the past contribute to the nonlinear phase shift affecting the pulse at a given instant. It can be written as the sum of an instantaneous contribution from the electronic response via a delta function and a delayed Raman response due to lattice vibrations as

$$R(T_{delay}) = (1 - f_R)\delta(T_{delay}) + f_R h_R(T_{delay}), \quad (7.2)$$

where $0 \leq f_R \leq 1$ is a scalar that determines the relative magnitude of the two contributions. The exact functional form of the Raman response function, $h_R(T_{delay})$,

depends on the material, but generally resembles a sine function multiplied by a dampening term and must satisfy $\int_{-\infty}^{\infty} h_R(T_{\text{delay}})dT_{\text{delay}} = 1$, as it essentially "weighs" how much the powers at different times in the past contribute to the current nonlinear phase shift. Additionally, it must be demanded that $h_R(T_{\text{delay}}) = 0$ for $T_{\text{delay}} \leq 0$ to prevent the expression from violating causality by letting *future* powers affect the current nonlinear phase shift. See [this interactive graph](#) for an illustration of the impact of past power on the phase shift caused by the Raman effect. Intuitively, the function $h_R(T_{\text{delay}})$ is like the function that describes the amplitude of a sound wave from a tuning fork, piano key or guitar string after it is suddenly struck; an oscillation that gradually "rings down". Continuing the analogy, if one views $|\mathbf{A}(z, T - T_{\text{delay}})|^2$ as a large collection of instantaneous strikes with different strengths at different times, it makes sense that the current oscillation depends on all the ones that were present in the past. Substituting Eq. 7.2 into Eq. 7.1 and evaluating the integral over the delta function yields

$$\partial_z \mathbf{A} = i\gamma \mathbf{A} \left((1 - f_R) |\mathbf{A}(z, T)|^2 + f_R \int_0^{\infty} h_R(T_{\text{delay}}) |\mathbf{A}(z, T - T_{\text{delay}})|^2 dT_{\text{delay}} \right). \quad (7.3)$$

Note that if the change in the power of the pulse is very slow compared to the duration of the response function, one can approximate $h_R(T_{\text{delay}}) \approx \delta(T_{\text{delay}})$ (or, equivalently, $|\mathbf{A}(z, T - T_{\text{delay}})|^2 \approx |\mathbf{A}(z, T)|^2$), in which case Eq. 5.1 is recovered. In other words, the Raman effect is only noticeable for pulses whose durations are close to the duration of the natural oscillations of the molecular lattice! Assuming that the pulse duration is noticeably longer than the duration of $h_R(T_{\text{delay}})$, so that its power for different time delays can be found by linearly extrapolating the present power and its gradient into the past, the integral in Eq. 7.3 can be written as

$$\begin{aligned} f_R \int_0^{\infty} h_R(T_{\text{delay}}) |\mathbf{A}(z, T - T_{\text{delay}})|^2 dT_{\text{delay}} &\approx \quad (7.4) \\ f_R \int_0^{\infty} h_R(T_{\text{delay}}) [|\mathbf{A}(z, T)|^2 - T_{\text{delay}} \partial_T |\mathbf{A}(z, T)|^2] dT_{\text{delay}} &= \\ |\mathbf{A}(z, T)|^2 f_R - \partial_T |\mathbf{A}(z, T)|^2 f_R \int_0^{\infty} T_{\text{delay}} h_R(T_{\text{delay}}) dT_{\text{delay}} &= \\ |\mathbf{A}(z, T)|^2 f_R - \partial_T |\mathbf{A}(z, T)|^2 T_R, \end{aligned}$$

where T_R is the average duration of the Raman response function scaled by f_R . Substituting the result of Eq. 7.4 into Eq. 7.3 yields

$$\partial_z \mathbf{A} = i\gamma \mathbf{A} (|\mathbf{A}(z, T)|^2 - T_R \partial_T |\mathbf{A}(z, T)|^2), \quad (7.5)$$

which contains the "usual" SPM term proportional to the current power and an additional term that depends in the time derivative of the power. For silica, $T_R \approx 3$ fs, so Eq. 7.5 will be valid for pulses longer than approximately 600 fs. The approximation applied in Eq. 7.4 could be extended to include the second derivative of $|A(z, T)|^2$ for increased accuracy. Recall from Eq. 5.3 and Fig. 5.1 that the "constant" SPM term causes a large decrease in the instantaneous frequency where the *derivative* of the power is very positive. By the same logic, the Raman term in Eq. 7.5 will cause a large decrease in the the instantaneous frequency where the "derivative of the derivative" is very negative. In other words, the Raman effect will tend to cause a red-shift at the peak of the pulse without an equivalently large blue-shift elsewhere, thus making the entire pulse "more red"! Physically, the red-shift arises because an incident photon can lose some of its energy by exciting mechanical vibrations in the crystal lattice of the medium.

7.1.1 Expressions for $h_R(T_{\text{delay}})$

An approximate expression for the Raman effect in silica, which assumes that the molecular vibrations are dominated by a single frequency is

$$h_R^{\text{basic}}(T_{\text{delay}}) = \left(\frac{1}{\tau_1^2} + \frac{1}{\tau_2^2} \right) \tau_1 \exp \left(-\frac{T_{\text{delay}}}{\tau_2} \right) \sin \left(\frac{T_{\text{delay}}}{\tau_1} \right), \quad (7.6)$$

with $f_R = 0.18$, $\tau_1 = 12.2$ fs and $\tau_2 = 32$ fs. All presented expressions for $h_R(T_{\text{delay}})$ are assumed to be zero for $T_{\text{delay}} \leq 0$ to respect causality. Mathematically, this can be ensured through multiplication by the Heaviside step-function. A more accurate approximation than Eq. 7.6 to the vibrational behavior of silica is

$$h_R^{\text{better}}(T_{\text{delay}}) = (1 - f_b) h_R^{\text{basic}}(T_{\text{delay}}) + f_b \frac{2\tau_b - T_{\text{delay}}}{\tau_b^2} \exp \left(-\frac{T_{\text{delay}}}{\tau_b} \right), \quad (7.7)$$

where $f_R = 0.245$, $f_b = 0.21$ and $\tau_b = 96$ fs. The exact expression for the Raman response of silica is

$$h_R^{\text{exact}}(T_{\text{delay}}) = c_{\text{norm}}^{-1} \sum_{n=0}^{12} C_n \exp \left(-g_n T_{\text{delay}} - 0.25 G_n^2 T_{\text{delay}}^2 \right) \sin \left(2\pi\nu_n T_{\text{delay}} \right), \quad (7.8)$$

where $f_R = 0.18$ and the parameters C_n , g_n , G_n , and ν_n are listed in Tab. 7.1.1 and $c_{\text{norm}} = 3.75225$ ps so that $\int_0^\infty h_R^{\text{exact}}(T_{\text{delay}}) dT_{\text{delay}} = 1$. A visualization of these three models of the Raman response of silica and their impacts on the same optical pulse is presented in Fig. 7.1. The imaginary parts of the Fourier Transforms of the

n	C_n	g_n [fs]	G_n [fs]	ν_n [THz]
0	1	0.521	1.562	1.69
1	11.4	1.163	3.310	3.00
2	36.67	1.749	5.246	6.93
3	67.67	1.624	4.872	10.87
4	74	1.352	4.057	13.88
5	4.5	0.245	0.734	14.90
6	6.8	0.415	1.244	18.33
7	4.6	1.549	4.647	20.74
8	4.2	0.594	1.784	23.79
9	4.5	0.642	1.928	25.05
10	2.7	1.499	4.497	27.88
11	3.1	0.909	2.728	32.38
12	3	1.599	4.797	36.42

Table 7.1: Table of parameters of the exact expression for the Raman response of silica in Eq. 7.8 modified from [1].

different expressions for $h_R(T_{delay})$ are plotted in Fig. 7.1 b). Physically, these spectra imply that the Raman effect allows a given optical frequency to "steal" power from frequencies 13 THz above it and forces it to "donate" power to frequencies 13 THz below it. For reasons similar to those addressed in Sec. 4.6, the real parts of the spectra (not shown) relate to the change in refractive index due to the Raman effect and allows one to determine the time delay it induces. From the maximum values of the curves shown in Fig. 7.1 b), the maximum Raman gain and thus the characteristic length over which the Raman effect becomes significant can be expressed as

$$g_{Raman} = \frac{4}{3}\gamma f_R P_0 n(\omega_0) \cdot \max(\text{Im}\{\mathfrak{F}\{h_R(T_{delay})\}(\omega)\}) \quad (7.9)$$

$$L_{Raman} = \frac{1}{g_{Raman}}, \quad (7.10)$$

where P_0 is the maximum power of the pulse and $n(\omega_0)$ is the refractive index of the medium (≈ 1.47 for silica). See [these video tutorials](#) for more information on the Raman effect.

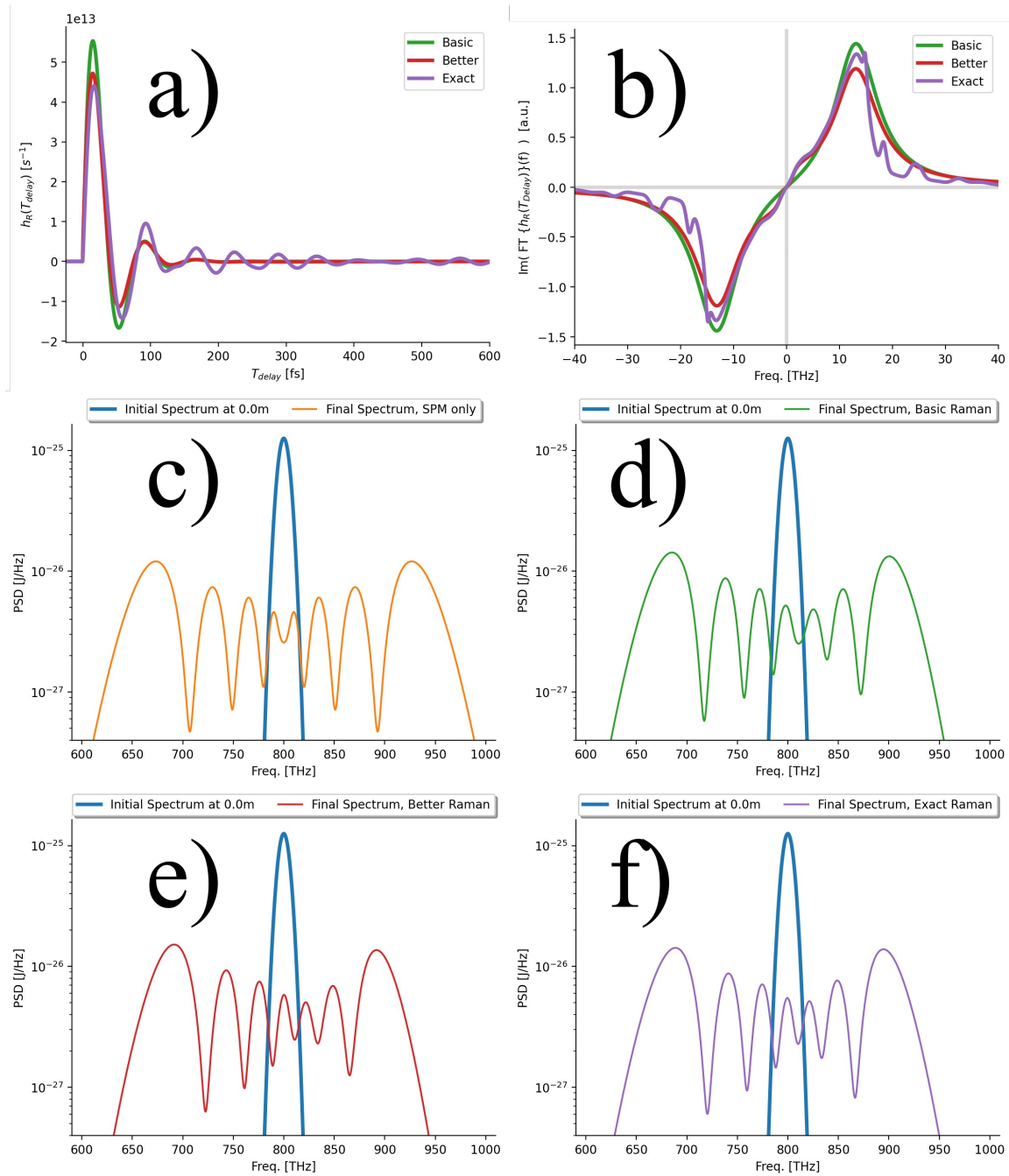


Figure 7.1: a) Graphs of Eq. 7.6 (green), Eq. 7.7 (red) and Eq. 7.8 (purple) in the time domain. b) Imaginary part of the Fourier Transform of the functions plotted in a). c) Initial and final spectrum of a pulse subjected to SPM only. d) Initial and final spectrum for the same pulse as in c) subjected to the Raman effect described by Eq. 7.6. Note the asymmetric broadening skewed to lower frequencies as predicted by the analysis of Eq. 7.5. e) Same as d) but for Eq. 7.7 f) Same as d) but for Eq. 7.8. Figures generated using [this interactive notebook](#), which the reader is encouraged to experiment with.

Chapter 8

Exotic pulses

For a fiber, where $\gamma \neq 0$ and $\beta_2 \neq 0$, a pulse launched into it can evolve in a number of surprising ways. Essentially, the nonlinearity will change the local frequency of the pulse based on its power profile, while dispersion will cause different frequencies to advance or delay relative to the carrier frequency, which in turn, alters the power profile. This chapter explores the interplay between these two effects for different values of γ and β_2 .

8.1 The Fundamental Soliton

Consider a fiber for which $\gamma > 0$. As illustrated in Fig. 5.1, this will cause leading(trailing) pulse edges to develop a red(blue) shift. As explained in Sec. 4.4, $\beta_2 < 0$ implies that blue light propagates faster than red light, thus causing the leading(trailing) edge of a pulse will become more blue(red). If $\gamma > 0$ makes the front(back) of the pulse more red(blue) based on the instantaneous power profile, while $\beta_2 < 0$ makes the front(back) more blue(red) according to the 2nd time derivative of the field, it's natural to ask if there exists a pulse envelope, where the two effects balance exactly at every instant, so that the shape of the pulse is unaltered as it propagates forward. For such a pulse, the field envelope should be independent of distance, while the phase should be independent of time, such that

$$\textcolor{red}{A}(z, T) = V(T)e^{i\phi(z)} \quad (8.1)$$

solves

$$\partial_z \textcolor{red}{A} = -i\frac{\beta_2}{2}\partial_T^2 \textcolor{red}{A} + i\gamma|\textcolor{red}{A}|^2 \textcolor{red}{A}. \quad (8.2)$$

As explained in [this derivation](#), it can be shown that the solution is

$$A(z, T) = \sqrt{\frac{|\beta_2|}{\gamma T_0^2}} \cdot \operatorname{sech} \left(\frac{T}{T_0} \right) \exp \left(i \frac{|\beta_2|}{2T_0^2} z \right), \quad (8.3)$$

where T_0 is the time at which the field of the pulse has decreased to 64.8% of its peak value. This stable pulse characterized by a hyperbolic secant envelope is referred to as a "fundamental soliton". See Fig. 8.1 for a comparison of a Gaussian pulse to a hyperbolic-secant pulse. Note that the peak power of the hyperbolic-secant pulse, A_{max} , must be chosen to exactly equal the characteristic amplitude, $A_{char} = \sqrt{|\beta_2|/\gamma T_0^2}$, for stable propagation to occur!

8.1.1 Solitons in telecommunications

As $\gamma > 0$ and $\beta_2 < 0$ in silica fibers for near-infrared frequencies close to 193 THz (≈ 1550 nm), fundamental solitons were once of great interest in telecommunications because their resistance to dispersion and constant shape reduced inter-symbol interference. However, the same improvements in electronic dispersion compensation mentioned in Subsection 4.4.1 have rendered the use of solitons for optical fiber communication obsolete. Instead, pulses with a so-called "root-raised-cosine" field envelope are used.

8.2 Higher order Solitons

If the peak power of the hyperbolic secant pulse smaller than $P_{char} = |A_{char}|^2 = |\beta_2|/\gamma T_0^2$, the nonlinear effect will be too weak compared to dispersion for a fundamental soliton to form. The pulse will thus simply broaden in the time domain as it propagates forward. If the peak power is increased beyond P_{char} , the pulse will exhibit "oscillations" as it evolves. For the special case of A_{max} being an integer multiple of A_{char} , the oscillating soliton evolution will be particularly well-behaved. See Fig. 8.2 a-b) for an example of the temporal and spectral evolutions of a soliton for which $A_{max} = 3A_{char}$. See [this video tutorial](#) for more information on solitons in fibers.

8.2.1 Soliton fission

Fundamental- and higher order solitons can be seen as "fixed points" of Eq. 8.2. However, Eq. 8.2 itself is only an approximation to Eq. 1.1, which provides a more general description of the physics affecting the propagation of an optical pulse in a

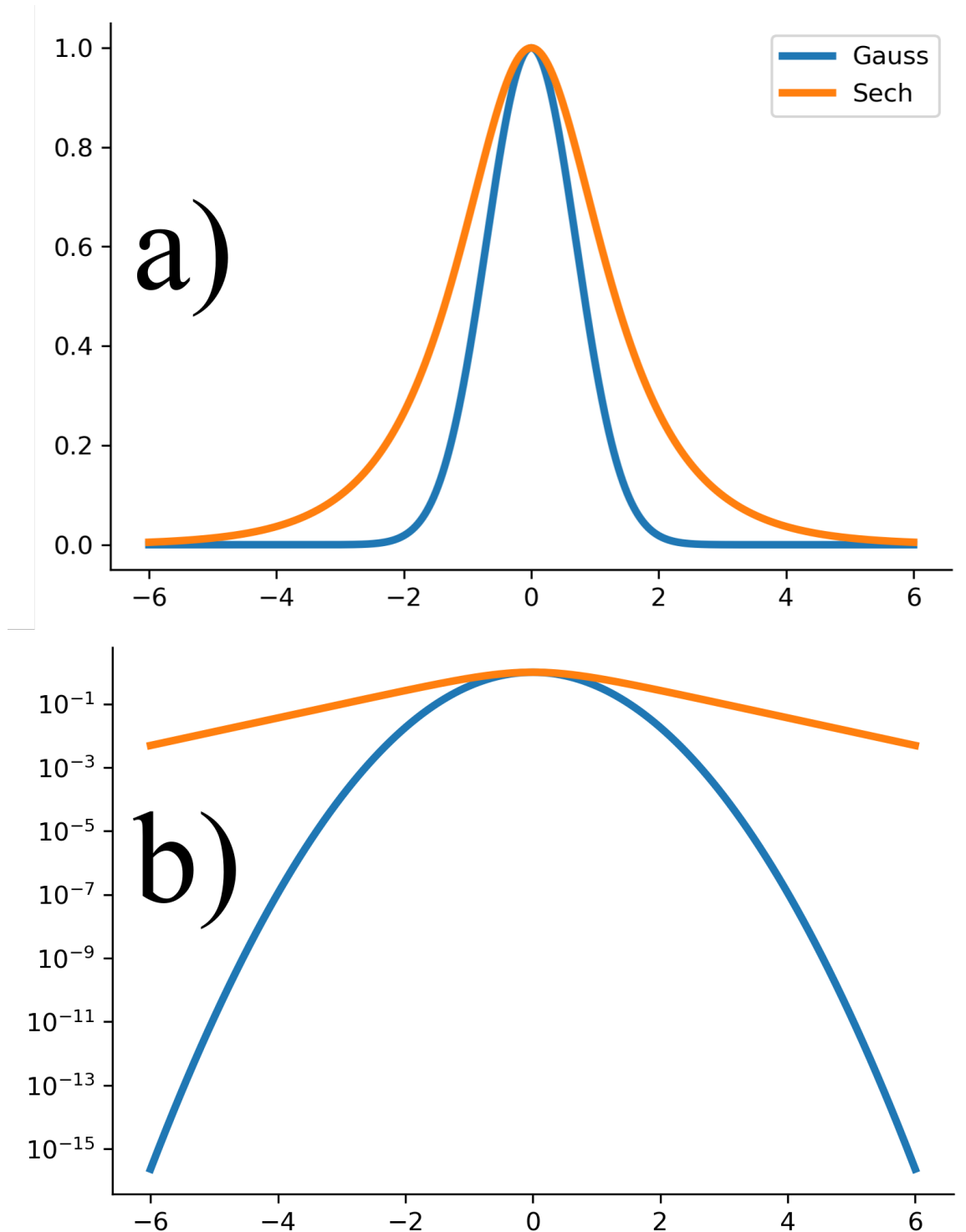


Figure 8.1: Comparison of a Gaussian pulse to a hyperbolic-secant pulse on a linear scale in a) and a logarithmic scale in b), which emphasizes the comparatively more intense tails of the hyperbolic-secant.

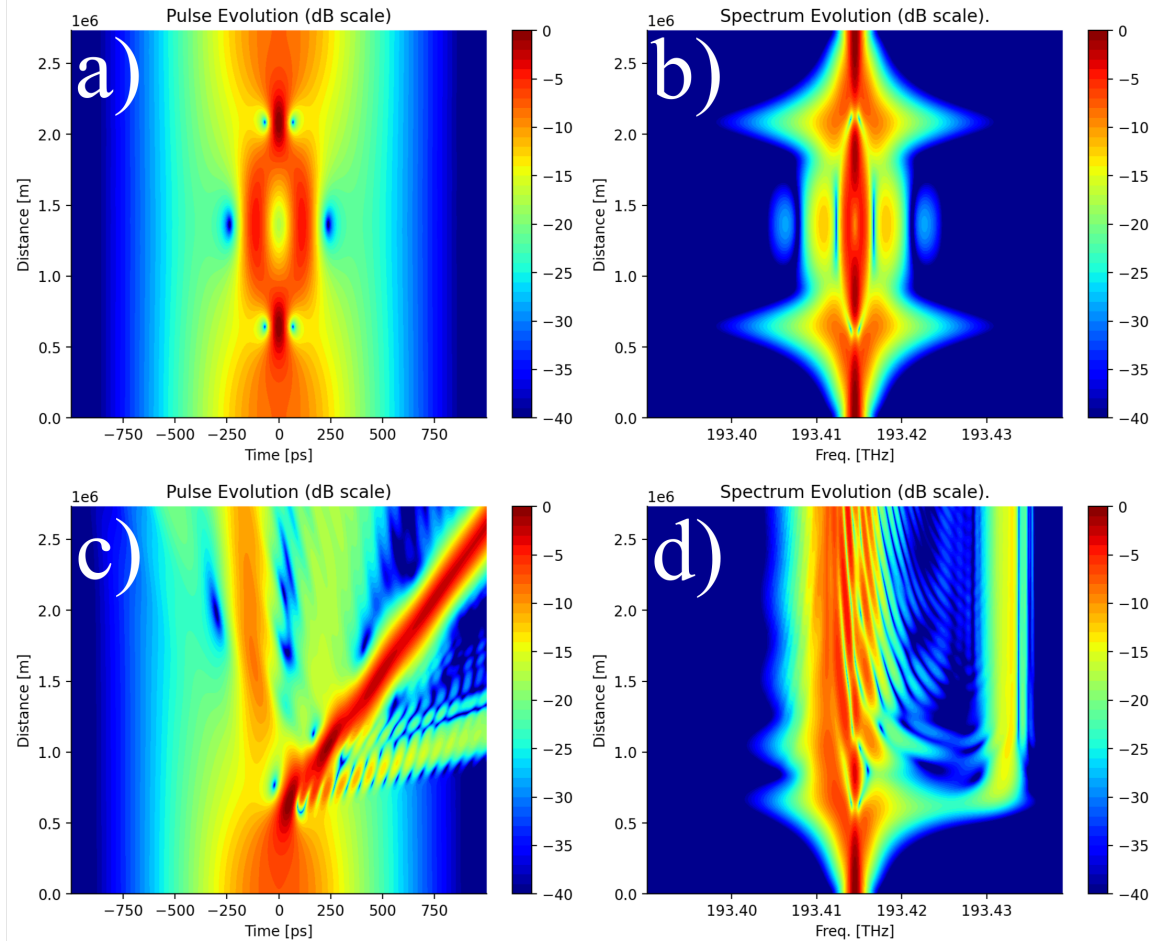


Figure 8.2: a) Temporal evolution of an $N = 3$ soliton for which $A_{max} = 3A_{char} = 3\sqrt{|\beta_2|/\gamma T_0^2}$. The length of the fiber has been chosen to equal the oscillation period of the soliton. b) Spectrum evolution of the $N = 3$ soliton. c-d) Respectively, the temporal and spectral evolutions of the same $N = 3$ soliton as in a-b), but where the fiber has $\beta_3 > 0$, causing the pulse to "fission", thereby illustrating the unstable nature of solitonic propagation. Figures generated using the numerical simulation in [this interactive notebook](#), which the reader is encouraged to experiment with.

dispersive and nonlinear medium. It turns out that the presence of effects other than $\gamma > 0$ and $\beta_2 < 0$ will eventually disturb the evolution of an initially solitonic pulse. In Fig. 8.2 c-d), the presence of $\beta_3 > 0$ causes a higher order soliton to "fission" into two less powerful ones at new frequencies due to FWM after propagating a distance of 0.5 meters. Other effects, such as Self-Steepening, the Raman effect or even Modulation Instability caused by optical noise propagating along with an otherwise ideal soliton pulse can similarly give rise to soliton fission. Thus, much like a pencil balanced on its tip, solitonic propagation should be viewed as an unstable equilibrium. See [this video tutorial](#) for more details on soliton fission.

8.3 Optical Wave Breaking

When an ocean wave approaches a beach, water begins to "pile up" on its leading edge, eventually causing the wave to "break" before crashing onto the shore. A similar phenomenon can be observed with optical waves in nonlinear fibers where $\gamma > 0$ and $\beta_2 > 0$. Instead of the local color-changes from nonlinearity and dispersion balancing as in Sec. 8.1 when β_2 was negative, they now "cooperate". The nonlinearity makes the front(back) of the pulse more red(blue) and dispersion causes red(blue) light to move faster(slower) than the carrier. The result is that any pulse will quickly broaden in the time domain. Often, this happens in such a way that power gradually "piles up" in both the front and back of the pulse, leading to steeper power slopes, which generate even larger chirps causing more rapid temporal broadening due to dispersion. When the slope steepness gets sufficiently large, dispersion will "launch" the newly generated frequencies away from the main pulse in a manner analogous to a crashing water wave. Figure 8.3 a-b) illustrates this effect called "Optical Wave Breaking" (OWB). While the changes to incident pulses induced by OWB can be detrimental, they can also be beneficial if one desires an optical pulse with steep slopes and approximately constant peak power. See [this video tutorial](#) for further details on OWB.

8.3.1 Similaritons

When $\gamma > 0$ and $\beta_2 > 0$, OWB broadens the pulse in the time domain, thereby reducing its peak power. If, additionally, $\alpha > 0$, implying that the pulse is amplified as it moves forward, this loss of peak power is continuously replaced. It turns out that under these circumstances, any input pulse *regardless of its initial shape* will evolve towards a parabolic power envelope as illustrated in Fig. 8.3 c) and a linearly changing chirp that goes from red in the front to blue in the back [20]. Both the peak power and duration of such a "similariton" will continuously increase with distance as explained in [this video tutorial](#). Similaritons can arise in certain optical amplifiers and their linearly changing chirps make them ideal candidates for generating pulses with extremely high peak powers through the Nobel-Prize winning method of chirped pulse compression explained in [this video tutorial](#).

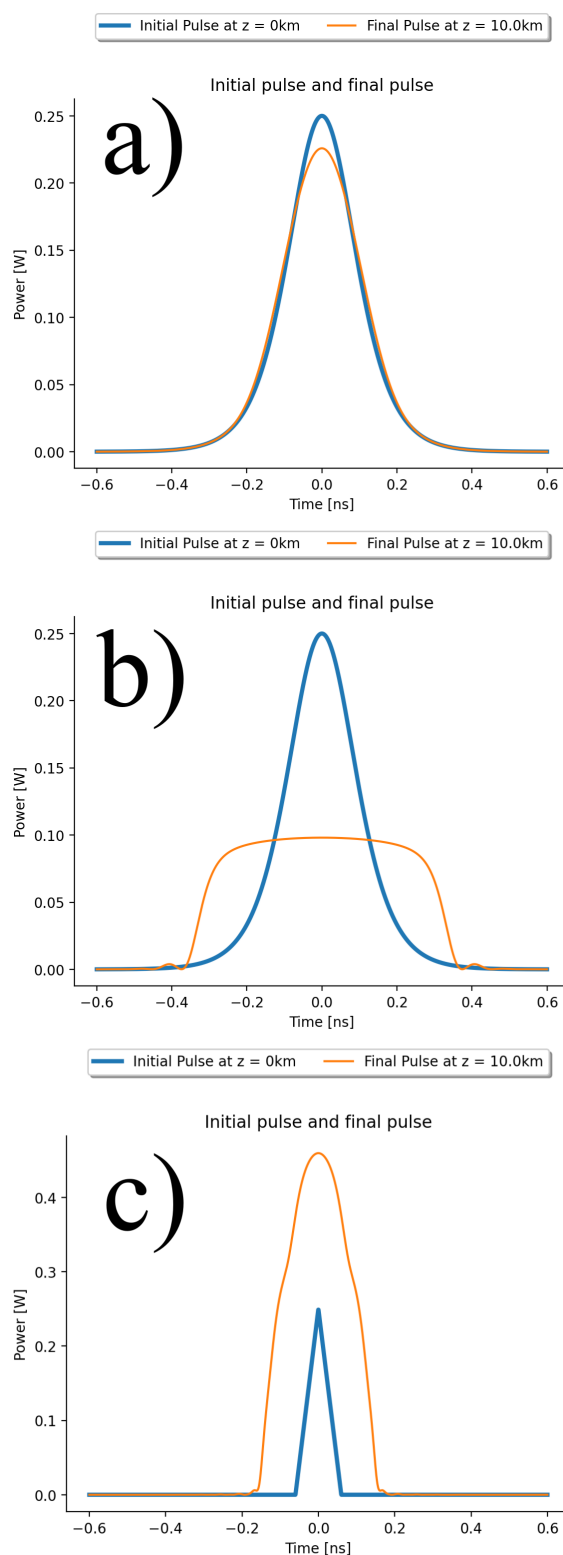


Figure 8.3: a) Evolution of a hyperbolic secant pulse through a medium where $\beta_2 > 0$. b) Evolution of the same pulse as in a) through a medium where $\beta_2 > 0$ and $\gamma > 0$ cause power to "pile up" in the front and back of the pulse, leading to OWB. c) Same conditions as in b), but where $\alpha > 0$ causes a triangular pulse to evolve towards a parabola. Figures generated using the numerical simulation in [this interactive notebook](#), which the reader is encouraged to experiment with.

8.4 Novel Solitons

8.4.1 Dark Solitons

Typically, optical pulses consist of a sudden increase in laser power preceded and followed by long durations of zero power. To the naked eye, such a pulse would be a bright flash, like a lamp being briefly switched on in a dark room. Such pulses can propagate stably through a nonlinear medium if the conditions described in Sec. 8.1 are satisfied. Consider instead what might be called an "anti-pulse" in a nonlinear medium; a high power CW signal, which experiences a brief dip in its power, analogous to a bright lamp that is briefly switched off before being reactivated. It will consist of a decreasing leading edge and an increasing trailing edge. If $\gamma > 0$ and $\beta_2 > 0$, the leading(trailing) edge becomes more blue(red), causing the light there to slow down(speed up). Similarly to Sec. 8.1, one can calculate that the field envelope for which nonlinearity and dispersion cancel exactly is a hyperbolic tangent, thereby leading to a stably propagating "Dark Soliton" described by

$$A(z, T) = A_{char} \tanh\left(\frac{T}{T_0}\right) \exp\left(i \frac{|\beta_2|}{T_0^2} z\right). \quad (8.4)$$

See [this video tutorial](#) for more information on Dark Solitons.

8.4.2 Raman Solitons

If the Raman effect, which shifts the spectrum of a pulse towards lower frequencies, is present in a nonlinear medium where $\beta_2 < 0$, a "Raman Soliton" can form. This soliton retains the shape of its envelope, but undergoes a constant red-shift and obtains an increasingly large time delay since $\beta_2 < 0$ implies that red light moves more slowly than blue light as illustrated in Fig. 8.4c-d). Raman solitons often arise after soliton fission of pulses with durations on the scale of tens of femtoseconds. See [this video tutorial](#) for an explanation of Raman solitons.

8.4.3 Vector Solitons

In Sec. 6.3, it was shown that two distinct frequencies of light can affect each others phases through the nonlinearity. Similarly, two different polarizations of light propagating in a nonlinear medium can affect each other's phases. Using a vectorial version of Eq.1.1 where $\gamma > 0$, $\beta_2 < 0$, and where the refractive index is different for light polarized along the x- and y-axes of the medium, one can obtain analytical expressions

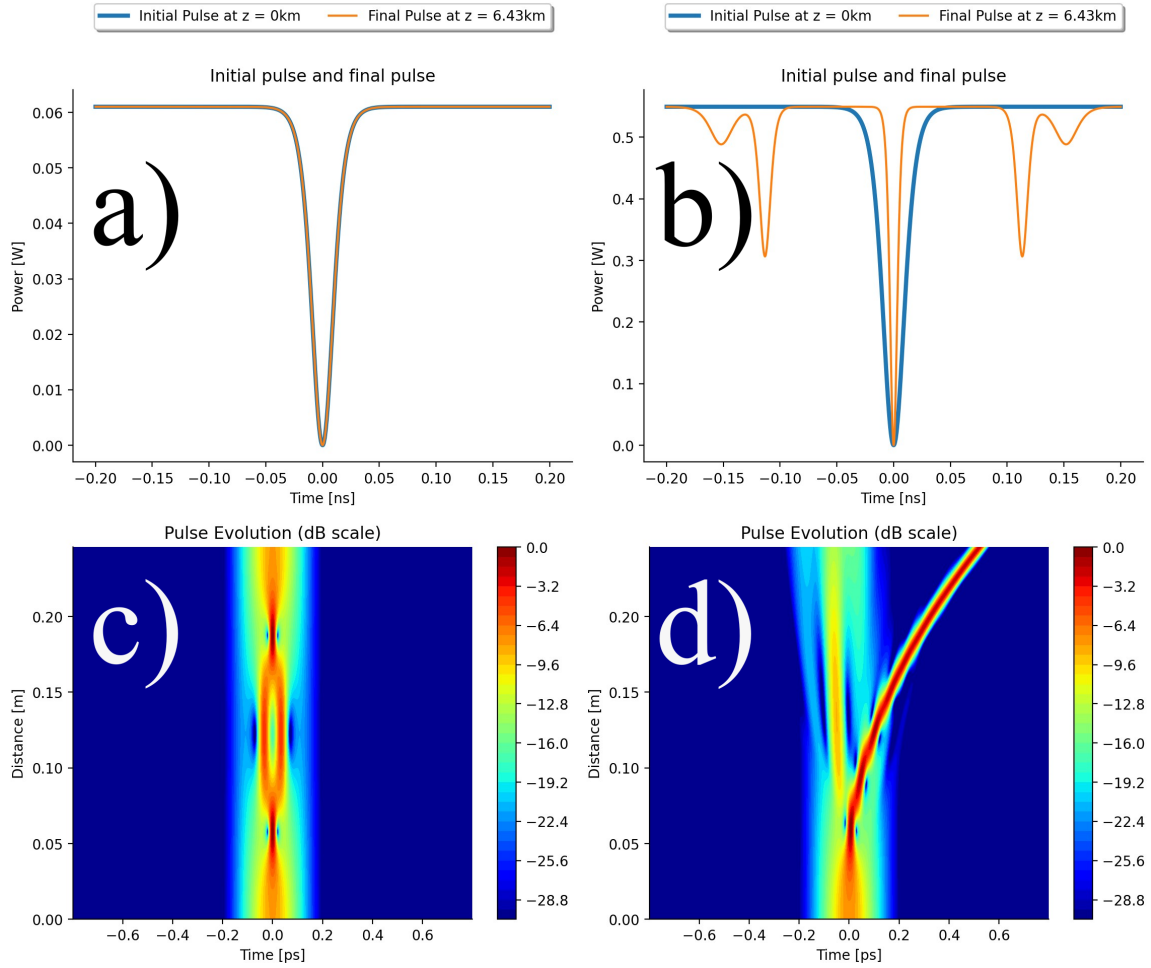


Figure 8.4: a) Fundamental dark soliton propagating stably through a medium where $\beta_2 > 0$ and $\gamma > 0$. b) An N=3 dark soliton propagating through the same medium as in a) Instead of stable propagation, the central dip gives rise to additional ones. c) An N=3 soliton propagating through a medium where $\beta_2 < 0$ and $\gamma > 0$. d) The same pulse as in c) propagating through the same medium except the Raman effect described by Eq. 7.6 is taken into account, causing soliton fission and a self-redshifting Raman soliton to arise. Figures generated using [this interactive notebook](#), which the reader is encouraged to experiment with.

for so-called "Vector Solitons". The special cases for which this is possible turn out to be circularly polarized light and light polarized linearly at 45° to the x-axis [21].

Chapter 9

Supercontinuum Generation

Previous chapters explained individual linear and nonlinear effects and the interplay of a limited number of them. A summary of their impacts is provided in Tab. 9.1. For high power pulses with carrier frequencies where $\beta_2 \lesssim 0$ and $\gamma > 0$ for a given medium as well as durations below approximately 100 fs, all of the listed effects may be present simultaneously. In this case, the evolution of the pulse may be highly non-trivial and broaden its spectrum by ten to twenty times its initial bandwidth [3]. This chapter presents an example of supercontinuum generation and explains how this process can be understood in terms of the previously presented effects.

9.1 Case study

To simulate the generation of a supercontinuum, the values in Tab. 9.2 were used. The resulting supercontinuum is presented in Fig. 9.1. The spectrum in Fig. 9.1 c) indicates that the pulse undergoes SPM during the first 1 m of propagation, while Fig. 9.1 b) indicates that soliton fission occurs immediately afterwards. The high-power pulse with a much smaller duration that walks off parabolically towards later times is a Raman soliton that continuously red-shifts itself. The low-power light that "walks off" linearly towards later times is most likely FWM generated when the fissioned soliton overlaps with the remnants of the initial pulse. See [this video tutorial](#) for an in-depth analysis of the properties of this supercontinuum.

9.2 Your turn!

To further explore the properties of the supercontinuum modelled in Fig. 9.1, open the [notebook](#) used for generating it, try the following experiments and explain how/why the evolution of the pulse and its spectrum are different. Before starting any ex-

Effect	Time domain	Spectrum	Significant for	Relevance
$\alpha > 0$	Increase power.	Increase power.	Amplifiers	NL effects highly power dependent.
$\beta_2 < 0$	Broadening with blue(red) light in front(back).	Quadratic change in phase with distance from carrier freq.	Short NIR pulses in silica.	NL effects significant when $\beta_2 + \gamma P \approx 0$.
β_3	Delays or advances non-carrier freqs. depending on sign.	Cubic change in phase with distance from carrier freq.	Carrier freqs. close to ZDF.	Different freqs. overlapping in time domain cause FWM. Soliton fission.
Self Phase Modulation	Red(blue)-shift on leading(trailing)edges.	Symmetric broadening.	High power pulses	Most basic NL effect. First to "kick in" as power is increased.
Self Steepening	Pulse peak delayed to later times causing steep back slope.	Broadening skewed towards higher frequencies.	Pulses with short duration compared to carrier freq.	Small correction on top of SPM. Soliton fission.
Raman	Red-shift at pulse peak.	Broadening skewed towards lower frequencies.	Extremely short pulses on the scale of 10-100fs.	Raman red-shift can exceed SPM broadening. Soliton fission.

Table 9.1: Summary of the impacts of different linear and nonlinear effects.

Parameter	Value
N time points	2^{14}
Time resolution [fs]	1.8
Pulse type	Sech
Duration [fs]	166.79
Peak Power [W]	50
Carrier freq. [THz]	282.823 (=1060 nm)
α [dB/km]	0
β_2 [s^2/m]	-3.051721e-27
β_3 [s^3/m]	7.29029e-41
β_4 [s^4/m]	-1.08817e-55
β_5 [s^5/m]	2.8941e-70
β_6 [s^6/m]	4.8348e-89
β_7 [s^7/m]	-1.1464e-113
β_8 [s^8/m]	1.8802e-128
β_9 [s^9/m]	-1.5054e-143
γ [1/W/m]	0.09
Self-Steepening	ON
Raman model	Eq. 7.6

Table 9.2: Simulation parameters used for generating a supercontinuum taken from [2]

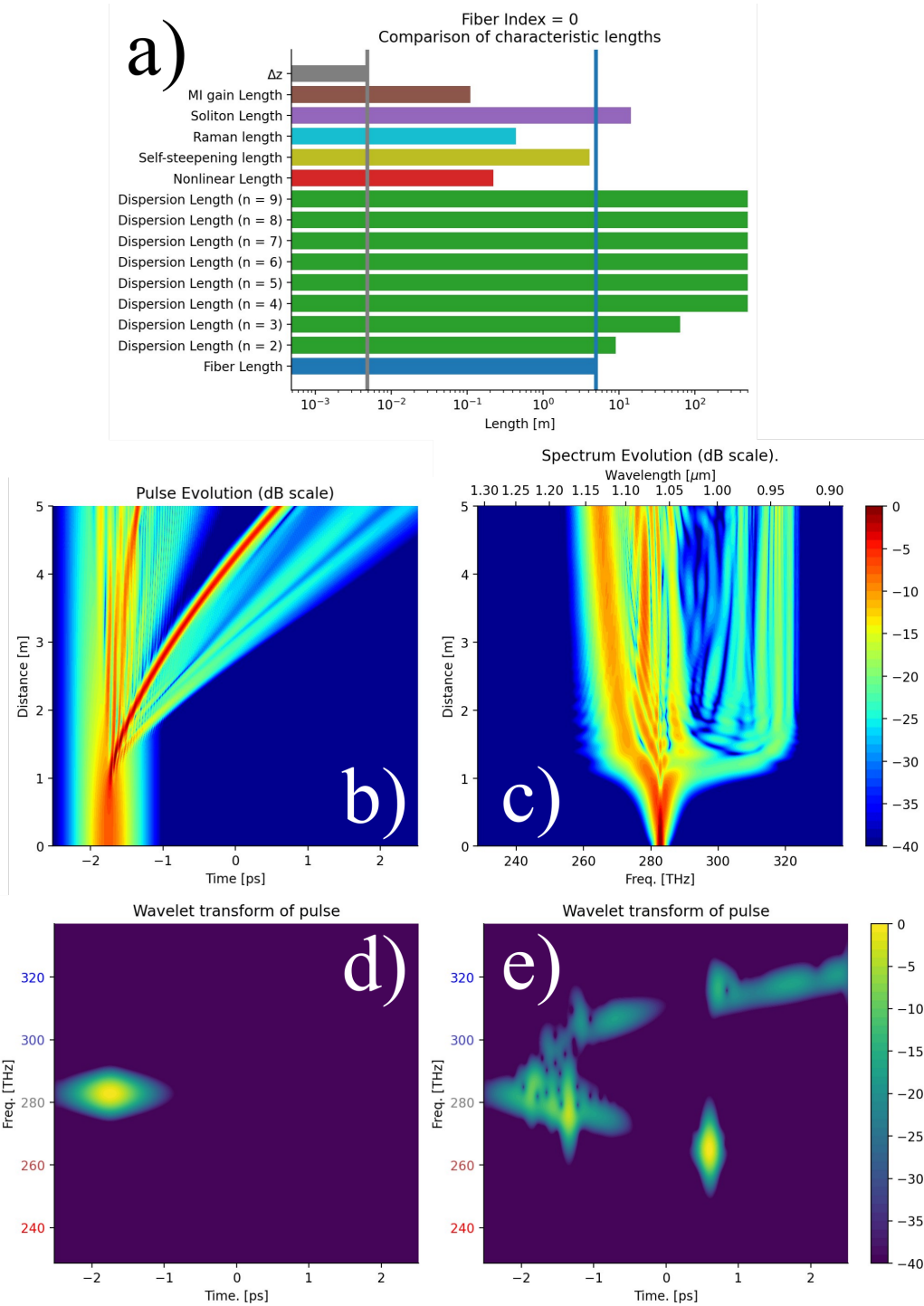


Figure 9.1: a) Comparison of the characteristic lengths resulting from the parameters listed in Tab. 9.2. Effects with short characteristic lengths are expected to become significant first. b) Temporal evolution of the pulse showing soliton fission at a distance of around 1 m followed by FWM and the generation of a Raman soliton walking off to later times. c) Spectral evolution of the pulse. d) Initial spectrogram of the pulse at $z=0$ m. e) Final spectrogram at $z=5$ m. The "parabolic" shape arises because $\beta_3 > 0$ ensures that both red and blue light experience time delays compared to the carrier. The bright spot at (0.75 ps, 265 THz) is a Raman soliton. Figures generated using the numerical simulation presented in [this interactive notebook](#), which the reader is encouraged to experiment with.

periment, write down a prediction of how you expect the simulation result to be altered, so you can compare with the actual result. Note that you should "reset" the parameters to the default values before each experiment:

1. **No nonlinearity.** The presented simulation uses $\gamma > 0$. Change this to $\gamma = 0$. Does the result indicate that nonlinearity has a large impact on the time evolution of the pulse?
2. **No Self-Steepening.** The presented simulation models the impact of self-steepening. Turn this effect off and asses if doing so had a significant impact.
3. **Negative α .** The presented simulation uses $\alpha = 0$. Change this to $\alpha = -1 \text{ dB/m}$.
4. **Positive β_2 .** The presented simulation uses $\beta_2 < 0$. Change the sign of β_2 so it becomes positive.
5. **Only $\beta_2 < 0$.** The presented simulation uses $\beta_n \neq 0$ for $n > 2$. Set $\beta_n = 0$ for $n > 2$, run the simulation and explain why the evolution of the pulse and its spectrum has changed.
6. **Negative β_3 .** The presented simulation uses $\beta_3 > 0$. Change the sign of β_3 so it becomes positive. Note that you may want to change the sign of the time offset from -1.75 ps to $+1.75 \text{ ps}$ to ensure proper graphing of the time evolution. Can you explain why a Raman soliton does not arise when $\beta_3 < 0$? HINT: Compute the zero dispersion frequency using Eq. 4.14 and consider how it changes when the sign of β_3 is flipped.
7. **Alter the Raman model.** The presented simulation uses Eq. 7.6 to model the impact of the Raman effect. Follow the hints in the notebook and use Eq. 7.7, Eq. 7.8 or $f_R = 0$ instead.

Chapter 10

Recommended material

The following is a list of useful and accessible resources on both optics, electronics and communication.

10.1 Optics

Elements of Photonics

This textbook by prof. Keigo Iizuka on the theory behind practical optical devices covers a wide range of topics. Highly recommended for its treatment of the gain and noise properties of the Erbium Doped Fiber Amplifier (EDFA), which is an essential instrument in modern optics and telecommunications.

Modern Optics lectures by Prof. Partha Roy Chaudhuri

This [free series of 60 video lectures](#) covers the basics of Maxwell's Equations, polarization and birefringence as well as more advanced topics including wave guides and devices such as electro-optical modulators. Highly recommended for the well-structured and mathematically thorough treatment of all described subjects.

Non-linear Optics lectures by Prof. Samudra Roy

This [series of 60 video lectures](#) first explains essential concepts in linear optics followed by a detailed derivation of both 2nd-order and 3rd-order nonlinear effects starting from Maxwell's Equations. Second Harmonic Generation (SHG), Difference Frequency Generation (DFG), Optical Parametric Oscillators (OPO) along with other phenomena beyond the scope of this primer are covered. Particularly recommended for its explanation of the symmetry- and tensor properties of the $\chi^{(2)}$ and $\chi^{(3)}$ nonlinearities.

Nonlinear Fiber Optics

This textbook by Govind P. Agrawal explains the mathematics behind Eq. 1.1 in great detail and with frequent reference to experimental results. Highly recommended for its in-depth treatment of advanced phenomena involving polarization, Stimulated Brillouin Scattering and novel fibers.

MIT "Demonstrations in Lasers and Optics" lecture series

Presented by prof. Shaoul Ezekiel, [this series of 49 video lectures](#) contains practical demonstrations of fundamental optical effects, such as polarization, interference and diffraction in the context of free-space optics. Highly recommended for its systematic experiments.

International School on Parametric Non Linear Optics lectures

This [series of 44 video lectures](#) delivered by experts in nonlinear optics. Highly recommended for covering advanced topics beyond what is usually described in ordinary course work.

Les' Lab

This [YouTube channel](#) specializes in practical demonstrations of laser-technology, including dye lasers, spectrometers, electro-optical modulators, SHG and even supercontinuum generation. Highly recommended for the illustrative demonstrations of relevant effects and the detailed explanations of the electronics required to operate optical devices.

YourFavouriteTA

This [YouTube channel](#) by the author of this primer explains nonlinear optics through both practical experiments, theoretical derivations and numerical simulations. It aims to provide intuitive explanations of both linear and nonlinear processes usually described by intricate equations.

10.2 Electronics

The Signal Path

This [YouTube channel](#) is dedicated to practical experiments, tear-downs and repairs of power supplies, signal generators, detectors, oscilloscopes, spectrum analyzers and

other equipment commonly found in scientific and industrial laboratories. Particularly recommended for its videos on Radio-Frequency (RF) devices.

EMPossible

This [YouTube channel](#) focuses on both the basics of electromagnetic theory and advanced topics such as RF waveguides, semi-conductor band structures and finite element analysis. Highly recommended for the broad range of concepts covered and the streamlined tutorials with excellent illustrations.

Keysight Electronics Tutorials

The [YouTube Channel](#) of the electronics equipment company, Keysight, contains explanations focusing on measurements of electrical signals. Highly recommended for the focus on oscilloscopes as this is a commonly used tool for visualizing the power over time measured by photodiodes.

Rohde&Schwarz Electronics Tutorials

This [YouTube playlist](#) produced by the electronics equipment company, Rohde&Schwarz, provides in-depth tutorials on measurement and characterization of properties of electrical devices and signals, such as power, phase noise, amplifier noise factor and more. Many of these concepts are highly transferable to the field of optics.

10.3 Communication

Ian Explains

This [YouTube channel](#) explains essential methods in digital and analog signal processing, communication and statistics. Highly recommended for its illustrative examples and straight-forward derivations.

10.4 Simulation tools

Octave Photonics

This free, interactive, [browser based tool](#) for solving Eq. 1.1 is great for visualizing the impact of essential phenomena like dispersion, soliton formation and the Raman effect. Highly recommended for its easy-to-use interface.

ssfm_functions.py

This [open-source python library](#) for solving Eq. 1.1 is created and maintained by the author of this primer. It provides a high degree of flexibility and customizability in setting up simulations using code. For example, arbitrary fiber links consisting of multiple spans with varying properties including different Raman models, input/output gain or dispersion compensation can be created using a for-loop, and simulation results are easily visualized using built-in plotting functions. The ability to modify the tool makes it ideal for graduate students in nonlinear optics, who often need to model novel and highly specific systems as part of their research.

gnlse-python

This [open-source python library](#) for solving Eq. 1.1 has excellent [documentation](#) and built-in visualization functions. An arXiv preprint explaining the implementation is also available [22].

GMMNLSE-Solver

This [open-source MATLAB library](#) allows one to solve a Multi-mode version of Eq. 1.1 and model exotic phenomena such as multi-mode solitons. It is a highly advanced tool recommended for extreme use-cases if one is already very comfortable with the basic single-mode case presented in this primer. If configured correctly, it allows computations to be parallelized on the GPU, making it quite fast for such a complex simulation.

Bibliography

- [1] Dawn Hollenbeck and Cyrus Cantrell. Multiple-vibrational-mode model for fiber-optic raman gain spectrum and response function. *Journal of the Optical Society of America B*, 19:2886, 12 2002. [doi:10.1364/JOSAB.19.002886](https://doi.org/10.1364/JOSAB.19.002886).
- [2] RuiFeng Chen, Kaiwen Yi, Yuanqiang Peng, Baoying Zou, and Weiyi Hong. The supercontinuum generation with pearcey-gaussian pulses in an optical fiber. *Results in Physics*, 18:103255, 2020. URL: <https://www.sciencedirect.com/science/article/pii/S2211379720317228>, [doi:10.1016/j.rinp.2020.103255](https://doi.org/10.1016/j.rinp.2020.103255).
- [3] R. R. Alfano and S. L. Shapiro. Observation of self-phase modulation and small-scale filaments in crystals and glasses. *Phys. Rev. Lett.*, 24:592–594, Mar 1970. URL: <https://link.aps.org/doi/10.1103/PhysRevLett.24.592>, [doi:10.1103/PhysRevLett.24.592](https://doi.org/10.1103/PhysRevLett.24.592).
- [4] R. Y. Chiao, E. Garmire, and C. H. Townes. Self-trapping of optical beams. *Phys. Rev. Lett.*, 13:479–482, Oct 1964. URL: https://www.researchgate.net/publication/220030032_Self-Trapping_of_Optical_Beams, [doi:10.1103/PhysRevLett.13.479](https://doi.org/10.1103/PhysRevLett.13.479).
- [5] Akira Hasegawa and Frederick Tappert. Transmission of stationary nonlinear optical pulses in dispersive dielectric fibers. I. Anomalous dispersion. *Applied Physics Letters*, 23(3):142–144, 08 1973. [arXiv:https://pubs.aip.org/aip/apl/article-pdf/23/3/142/18428001/142__online.pdf](https://arxiv.org/abs/https://pubs.aip.org/aip/apl/article-pdf/23/3/142/18428001/142__online.pdf), [doi:10.1063/1.1654836](https://doi.org/10.1063/1.1654836).
- [6] L. F. Mollenauer, R. H. Stolen, and J. P. Gordon. Experimental observation of picosecond pulse narrowing and solitons in optical fibers. *Phys. Rev. Lett.*, 45:1095–1098, Sep 1980. URL: <https://ieeexplore.ieee.org/document/1070843>, [doi:10.1103/PhysRevLett.45.1095](https://doi.org/10.1103/PhysRevLett.45.1095).
- [7] Pierluigi Poggolini, Gabriella Bosco, Andrea Carena, Vittorio Curri, Yanchao Jiang, and Fabrizio Forghieri. A detailed analytical derivation of the gn model

- of non-linear interference in coherent optical transmission systems, 2014. URL: <https://arxiv.org/abs/1209.0394>, arXiv:1209.0394.
- [8] O. Krarup. A Primer on the Nonlinear Schrödinger Equation. Commit SHA: 9f1b93a. URL: https://github.com/OleKrarup123/NLSE-primer/blob/main/NLSE_primer.pdf.
- [9] Donna Strickland and Gerard Mourou. Compression of amplified chirped optical pulses. *Optics Communications*, 56(3):219–221, 1985. URL: <https://www.sciencedirect.com/science/article/pii/0030401885901208>, doi:10.1016/0030-4018(85)90120-8.
- [10] Klaus Hentschel. Das Brechungsgesetz in der Fassung von Snellius. *Archive for History of Exact Sciences*, 55(4):297–344, January 2001. URL: https://www.academia.edu/20607033/Das_Brechungsgesetz_in_der_Fassung_von_Snellius, doi:10.1007/s004070000026.
- [11] J.B.J. Fourier. *Théorie analytique de la chaleur*. F.Didot, 1822. URL: https://archive.org/details/bub_gb_TDQJAAAAIAAJ/page/n11/mode/2up.
- [12] J.B.J. Fourier. *Analytical Theory of Heat*. Cambridge University Press, 1878. URL: <https://www3.nd.edu/~powers/ame.20231/fourier1878.pdf>.
- [13] S.E. Mechels, J.B. Schlager, and D.L. Franzen. Accurate measurements of the zero-dispersion wavelength in optical fibers. *Journal of Research of the National Institute of Standards and Technology*, 102(3):333, May 1997. URL: <https://nvlpubs.nist.gov/nistpubs/jres/102/3/j23mec.pdf>, doi:10.6028/jres.102.023.
- [14] NIST Digital Library of Mathematical Functions. <http://dlmf.nist.gov/10.12>, Release 1.0.27 of 2020-06-15. F. W. J. Olver, A. B. Olde Daalhuis, D. W. Lozier, B. I. Schneider, R. F. Boisvert, C. W. Clark, B. R. Miller, B. V. Saunders, H. S. Cohl, and M. A. McClain, eds. URL: <http://dlmf.nist.gov/10.12>.
- [15] A. Boskovic, S. V. Chernikov, J. R. Taylor, L. Gruner-Nielsen, and O. A. Levring. Direct continuous-wave measurement of n₂ in various types of telecommunication fiber at 1.55 μm. *Opt. Lett.*, 21(24):1966–1968, Dec 1996. doi:10.1364/OL.21.001966.
- [16] Ole Krarup. *Enhancement of Fiber Optical Environmental Sensor Performance Via All-Optical Signal Processing*. PhD thesis, University of Ottawa, 03 2024. URL: <https://doi.org/10.20381/ruor-30193>.

- [17] Benoit Vanus. *All-Optical Signal Processing Using the Kerr Effect for Fiber-Based Sensors*. PhD thesis, University of Ottawa, 10 2021. URL: <https://ruor.uottawa.ca/handle/10393/42827?mode=full>.
- [18] Yang Lu. *Study of the Kerr Phase-Interrogator and Its Applications*. PhD thesis, University of Ottawa, 11 2015. URL: <https://ruor.uottawa.ca/handle/10393/33376?mode=full>.
- [19] C. V. Raman. A new radiation [reproduced from indian j. phys., 1928, 2, 387–398]. *Current Science*, 74(4):382–386, 1998. URL: <http://www.jstor.org/stable/24101519>.
- [20] Vladimir I. Kruglov and John D. Harvey. Asymptotically exact parabolic solutions of the generalized nonlinear schrödinger equation with varying parameters. *J. Opt. Soc. Am. B*, 23(12):2541–2550, Dec 2006. URL: https://www.academia.edu/73198213/Asymptotically_exact_parabolic_solutions_of_the_generalized_nonlinear_Schr%C3%B6dinger_equation_with_varying_parameters, doi:10.1364/JOSAB.23.002541.
- [21] Govind Agrawal. Chapter 6 - polarization effects. In Govind Agrawal, editor, *Nonlinear Fiber Optics (Fifth Edition)*, Optics and Photonics, pages 193–244. Academic Press, Boston, fifth edition edition, 2013. doi:10.1016/B978-0-12-397023-7.00006-1.
- [22] Paweł Redman, Magdalena Zatorska, Adam Pawłowski, Daniel Szulc, Sylwia Majchrowska, and Karol Tarnowski. gnlse-python: Open source software to simulate nonlinear light propagation in optical fibers, 2021. URL: <https://arxiv.org/abs/2110.00298>, arXiv:2110.00298.